PHYSICAL REVIEW D **81,** 114004 (2010)

Forward-backward asymmetry of top quark pair production

Qing-Hong Cao,[1,2,*] David McKeen,[2,†] Jonathan L. Rosner,[2,‡] Gabe Shaughnessy,[1,3,§] and Carlos E. M. Wagner[1,2,4,‖]

[1]*HEP Division, Argonne National Laboratory, Argonne, Illinois 60439, USA*
[2]*Enrico Fermi Institute, University of Chicago, Chicago, Illinois 60637, USA*
[3]*Department of Physics and Astronomy, Northwestern University, Evanston, Illinois 60208, USA*
[4]*Kavli Institute for Cosmological Physics, University of Chicago, 5640 S. Ellis Avenue, Chicago, Illinois 60637, USA*

(Received 12 April 2010; published 3 June 2010)

We adopt a Markov chain Monte Carlo method to examine various new physics models which can generate the forward-backward asymmetry in top quark pair production observed at the Tevatron by the CDF Collaboration. We study the following new physics models: (1) exotic gluon G', (2) extra Z' boson with flavor-conserving interaction, (3) extra Z' with flavor-violating u-t-Z' interaction, (4) extra W' with flavor-violating d-t-W' interaction, and (5) extra scalars S and $S^{\pm}$ with flavor-violating u-t-S and d-t-$S^{\pm}$ interactions. After combining the forward-backward asymmetry with the measurement of the top pair production cross section and the $t\bar{t}$ invariant mass distribution at the Tevatron, we find that an axial vector exotic gluon G' of mass about 1 TeV or 2 TeV or a W' of mass about 2TeV offer an improvement over the standard model. The other models considered do not fit the data significantly better than the standard model. We also emphasize a few points that have been long ignored in the literature for new physics searches: (1) heavy resonance width effects, (2) renormalization scale dependence, and (3) next-to-leading order corrections to the $t\bar{t}$ invariant mass spectrum. We argue that these three effects are crucial to test or exclude new physics effects in the top quark pair asymmetry.

DOI: 10.1103/PhysRevD.81.114004 PACS numbers: 14.65.Ha

I. INTRODUCTION

The CDF Collaboration has observed a 2.3σ deviation in the forward-backward (F-B) asymmetry of top quark pair production at the Tevatron, using a data sample with 3.2 fb^{-1} integrated luminosity [1]:

$$A_{\rm FB}^{p\bar{p}}(\cos\theta) = 0.193 \pm 0.065(\text{stat}) \pm 0.024(\text{syst}). \quad (1)$$

This measurement improves the previous CDF result based on 1.9 fb^{-1} [2],

$$A_{\rm FB}^{p\bar{p}}(\cos\theta) = 0.17 \pm 0.08, \quad \text{and}$$
$$A_{\rm FB}^{t\bar{t}}(\Delta\eta) = 0.24 \pm 0.14,$$

where the results given in the lab ($p\bar{p}$) and the center-of-mass (c.m.) frame of the top quark pair ($t\bar{t}$) are consistent with the theoretically expected dilution of 30% in passing from $t\bar{t}$ to $p\bar{p}$ [3]. It is also consistent with the D0 result based on 0.9 fb^{-1} [4]:

$$A_{\rm FB}^{\rm obs} = 0.19 \pm 0.09(\text{stat}) \pm 0.02(\text{syst}), \quad \text{and}$$
$$A_{\rm FB}^{\rm obs} = 0.12 \pm 0.08(\text{stat}) \pm 0.01(\text{syst})$$

for exclusive 4-jet events and inclusive 4-jet events, respectively. Although the value is still consistent at a confidence level of $\sim$1.5% with the standard model (SM) prediction, which is [5,6]

$$A_{\rm FB}^{p\bar{p}}(\cos\theta) = 0.051 \pm 0.015, \quad (2)$$

it is interesting to ask whether or not the large central value can be explained by new physics (NP) after one takes into account other Tevatron experimental measurements of top quark pair production. There has been recent excitement among theorists for this measurement at the Tevatron [7–18].

In this work we point out that a strong correlation exists between $A_{\rm FB}$ and $\sigma(t\bar{t})$ measurements and further derive the bounds on NP from both measurements under the interpretation of a variety of models.

One should also keep in mind that, thanks to $p\bar{p}$ collisions, the Tevatron offers the best opportunity for measuring the asymmetry of top quark pair production, because of the basic asymmetry of the production process. At the LHC, the asymmetry of top quark pair production is an odd function of the pseudorapidity of the $t\bar{t}$ pair, due to the lack of definition of the forward direction. Hence, the LHC will improve the measurement of the total cross section of top quark pairs, but has very limited reach for studying the asymmetry. In this sense the Tevatron plays a unique role for testing top quark interactions, and it would provide more accurate measurements with future accumulated data. Projected bounds on both $A_{\rm FB}$ and $\sigma(t\bar{t})$ at the Tevatron with 10 fb^{-1} integrated luminosity are also presented.

The paper is organized as follows: In Sec. II, we examine the correlation between $A_{\rm FB}$ and $\sigma(t\bar{t})$ based on the recent Tevatron measurement, using the Markov chain

*caoq@hep.anl.gov
†mckeen@theory.uchicago.edu
‡rosner@hep.uchicago.edu
§g-shaughnessy@northwestern.edu
‖cwagner@hep.anl.gov

Monte Carlo (MCMC) method. We then give examples of a few interesting NP models generating the asymmetry, e.g., an exotic gluon G' (Sec. III), a model-independent effective field theory approach (Sec. IV), a flavor-conserving (FC) Z' boson (Sec. V), a flavor-violating (FV) Z' or W' (Sec. VI), and a new scalar $S(S^{\pm})$ (Sec. VII). We then conclude in Sec. VIII.

II. CORRELATION OF $A_{\rm FB}$ AND $\sigma(t\bar{t})$

The asymmetry $A_{\rm FB}$ in the top quark pair production can be parameterized as follows:

$$A_{\rm FB}^{\rm tot} = \frac{\sigma_F^{\rm SM} - \sigma_B^{\rm SM} + \sigma_F^{\rm NP} - \sigma_B^{\rm NP}}{\sigma_F^{\rm SM} + \sigma_B^{\rm SM} + \sigma_F^{\rm NP} + \sigma_B^{\rm NP}}, \tag{3}$$

$$= \frac{\sigma_F^{\rm NP} - \sigma_B^{\rm NP}}{\sigma_F^{\rm NP} + \sigma_B^{\rm NP}} \times \left(1 + \frac{\sigma_F^{\rm SM} - \sigma_B^{\rm SM}}{\sigma_F^{\rm NP} - \sigma_B^{\rm NP}}\right) \times \frac{\sigma_{\rm tot}^{\rm NP}}{\sigma_{\rm tot}^{\rm SM} + \sigma_{\rm tot}^{\rm NP}}, \tag{4}$$

$$= A_{\rm FB}^{\rm NP} \times R + A_{\rm FB}^{\rm SM}(1 - R), \tag{5}$$

where

$$A_{\rm FB}^{\rm NP} \equiv \frac{\sigma_F^{\rm NP} - \sigma_B^{\rm NP}}{\sigma_F^{\rm NP} + \sigma_B^{\rm NP}}, \quad A_{\rm FB}^{\rm SM} \equiv \frac{\sigma_F^{\rm SM} - \sigma_B^{\rm SM}}{\sigma_F^{\rm SM} + \sigma_B^{\rm SM}} \quad \text{and} \quad R = \frac{\sigma_{\rm tot}^{\rm NP}}{\sigma_{\rm tot}^{\rm SM} + \sigma_{\rm tot}^{\rm NP}} \tag{6}$$

is the asymmetry induced by the NP, the asymmetry in the SM, and the fraction of the NP contribution to the total cross section, respectively. In this work we consider the case that the NP contribution to $A_{\rm FB}$ occurs in the process $q\bar{q} \to t\bar{t}$, for which the SM contributions do not generate any asymmetry at all at LO. However, at next-to-leading order (NLO) a nonzero $A_{\rm FB}^{\rm SM}$ is generated.

It is worth while emphasizing the factorization of $A_{\rm FB}^{\rm NP}$ and R in Eq. (5), as it clearly reveals the effects of NP on both the asymmetry and the top quark pair production cross section. For example, when NP effects generate a negative F-B asymmetry, they still produce a positive observed asymmetry as long as they give rise to a negative contribution to $\sigma(t\bar{t})$. This is important when the effects of interference between the SM QCD channel and the NP channel dominate. Moreover, the possibility of negative contributions to $\sigma_F^{\rm NP}$ or $\sigma_B^{\rm NP}$ means that $|A_{\rm FB}^{\rm NP}|$ can exceed 1.

Recently, the CDF Collaboration [19] published new results on the $t\bar{t}$ cross section in the lepton plus jet channels using a neural network analysis, based on an integrated luminosity of 4.6 fb^{-1},

$$\begin{aligned}
&\sigma(m_t = 171.0\ \text{GeV}) \\
&\quad = [8.33 \pm 0.40(\text{stat}) \pm 0.39(\text{sys}) \pm 0.17(\text{theo})]\ \text{pb}, \\
&\sigma(m_t = 172.5\ \text{GeV}) \\
&\quad = [7.63 \pm 0.37(\text{stat}) \pm 0.35(\text{sys}) \pm 0.15(\text{theo})]\ \text{pb}, \\
&\sigma(m_t = 175.0\ \text{GeV}) \\
&\quad = [7.29 \pm 0.35(\text{stat}) \pm 0.34(\text{sys}) \pm 0.14(\text{theo})]\ \text{pb},
\end{aligned} \tag{7}$$

and also an analysis combining leptonic and hadronic channels with an integrated luminosity of up to 4.6 fb^{-1} [20],

$$\begin{aligned}
&\sigma(m_t = 172.5\ \text{GeV}) \\
&\quad = [7.50 \pm 0.31(\text{stat}) \pm 0.34(\text{sys}) \pm 0.15(\text{theo})]\ \text{pb}.
\end{aligned} \tag{8}$$

Note that the theory uncertainty is derived from the ratio with respect to the Z cross section, and the central value is quoted after reweighting to the central values of the CTEQ6.6M parton distribution function (PDF) [21]. By means of the ratio with respect to the Z cross section, the luminosity-dependence of the theoretical $t\bar{t}$ cross section is replaced with the uncertainty in the theoretical Z boson production cross section. That reduces the total uncertainty to 7%, greatly surpassing the Tevatron Run II goal of 10%.

In this work we fix the top quark mass to be 175 GeV as we also include the the CDF measurement of the invariant mass spectrum of top quark pairs in our study, which is based on $m_t = 175$ GeV. We rescale the combined CDF measurements at $m_t = 172.5$ GeV [cf. Eq. (7)] to $m_t = 175$ GeV, which we estimate to be

$$\sigma(t\bar{t}) = [7.0 \pm 0.5]\ \text{pb}, \tag{9}$$

on the basis of the approximate behavior of Eqs. (7) and (8) and the theoretical calculation by Langenfeld, Moch, and Uwer [22]. It yields $|R| \leq 7\%$ at the 1σ level. Any asymmetry induced by the NP ($A_{\rm FB}^{\rm NP}$) is highly suppressed by the SM cross section due to the small fraction R; see Eq. (5).

A. Parameter estimation

In this work we utilize a MCMC to examine the correlation of $A_{\rm FB}$ and R. The MCMC approach is based on Bayesian methods to scan over specified input parameters given constraints on an output set. In Bayes' rule, the posterior probability of the model parameters, θ, given the data, d, and model, M, is given by

$$p(\theta|d, M) = \frac{\pi(\theta|M)p(d|\theta, M)}{p(d|M)}, \tag{10}$$

where $\pi(\theta|M)$ is known as the prior on the model parameters, which contains information on the parameters before unveiling the data. The $p(d|\theta, M)$ term is the likelihood

and is given below in Eq. (11). The $p(d|M)$ term is called the evidence, but is often ignored as the probabilities are properly normalized to sum to unity. In using the MCMC, we follow the Metropolis-Hastings algorithm, in which a random point, θ_i, is chosen in a model's parameter space and has an associated likelihood, $\mathcal{L}_i$, based on the applied constraints. A collection of these points, $\{\theta_i\}$, constructs the chain. The probability of choosing another point that is different than the current one is given by the ratio of their respective likelihoods: $\min(\frac{\mathcal{L}_{i+1}}{\mathcal{L}_i}, 1)$. Therefore, the next proposed point is chosen if the likelihood of the next point is higher than the current. Otherwise, the current point is repeated in the chain. The advantage of a MCMC approach is that in the limit of large chain length the distribution of points, θ_i, approaches the posterior distribution of the modeling parameters given the constraining data. In addition, the set formed by a function of the points in the chain, $f(\theta_i)$, also follows the posterior distribution of that function of the parameters given the data. How well the chain matches the posterior distribution may be determined via convergence criteria. We follow the method outlined in Ref. [23] to verify convergence after generating 25 000 unique points in the chain.

We adopt the likelihood

$$\mathcal{L}_i = e^{-\Sigma_j \chi_j^2/2} = e^{-\Sigma_j (y_{ij}-d_j)^2/2\sigma_j^2}, \tag{11}$$

where y_{ij} are the observables calculated from the input parameters of the ith chain, d_j are the values of the experimental and theoretical constraints and σ_j are the associated uncertainties. In our case, the input parameter set is taken to be $\theta_i = \{\sigma_{t\bar{t}}^{\rm SM}, \sigma_{t\bar{t}}^{\rm NP}, A_{\rm FB}^{\rm SM}, A_{\rm FB}^{\rm NP}\}$. We scan with flat priors for the unknown inputs with a range of

$$-5 \text{ pb} \le \sigma_{t\bar{t}}^{\rm NP} \le 5 \text{ pb} \qquad -5 \le A_{\rm FB}^{\rm NP} \le 5 \tag{12}$$

(recall that, as a result of its definition, $|A_{\rm FB}^{\rm NP}|$ may exceed 1), while the known inputs are scanned with normal distributions about their calculated central values,

$$\sigma_{t\bar{t}}^{\rm SM} = 6.38 \text{ pb} \pm 0.50 \text{ pb} \qquad A_{\rm FB}^{\rm SM} = 0.051 \pm 0.015. \tag{13}$$

The calculated total $t\bar{t}$ production cross section at NLO for $m_t = 175$ GeV has been taken as [24–26]

$$\sigma_{\rm th}(t\bar{t}) = 6.38^{+0.3}_{-0.7}(\text{scale})^{+0.4}_{-0.3}(\text{PDF}) \text{ pb}, \tag{14}$$

where the PDF uncertainty is evaluated using the CTEQ6.6M PDF [21]. The fully next-to-next-to-leading order (NNLO) QCD correction to top pair production is highly desirable to make a more reliable prediction on the asymmetry. Since it is still not clear how the asymmetry will be affected by the complete NNLO QCD corrections, we consider the NLO QCD corrections to the top quark pair production throughout this work without including the partial NNLO QCD corrections computed in [22,27,28]. However, it is conceivable that the asymmetry is not drastically affected with respect to the resummation in the partial NNLO results as was found in the resummation at NLO [29].

While both CDF and D0 have measurements of the invariant mass distribution [30,31], only CDF presents an unfolded differential cross section. Therefore, we inspected the $t\bar{t}$ invariant mass spectra reported by CDF; see Fig. 1. We take the seven bins with $M_{t\bar{t}} > 400$ GeV in our fit and weight their χ^2 by the number of included bins. This assigns an equal weight between the $M_{t\bar{t}}$ measurement and the $\sigma_{t\bar{t}}$ and $A_{\rm FB}$ measurements.

The observables are $d_i = \{\sigma(t\bar{t})^{\rm exp}, A_{\rm FB}^{\rm exp}\}$ in addition to the binned $\frac{d\sigma}{dM_{t\bar{t}}}$ data and define the output set. We use the combined cross section of Eq. (8). We therefore assign $d_i = \{7.00, 0.193\}$ and $\sigma_i = \{0.50, 0.069\}$ in our implementation of the likelihood defined above for the case we denote as "Current" ($\int \mathcal{L}dt = 4.6$ fb^{-1} for $\sigma_{t\bar{t}}$, $\int \mathcal{L}dt = 3.2$ fb^{-1} for $A_{\rm FB}$, and $\int \mathcal{L}dt = 2.7$ fb^{-1} for $\frac{d\sigma}{dM_{t\bar{t}}}$), while $d_i = \{7.00, 0.193\}$ and $\sigma_i = \{0.34, 0.039\}$ for the case we denote as "Projected," where $\int \mathcal{L}dt = 10$ fb^{-1} of integrated luminosity is used for each measurement, in which we assume the central values are fixed and the uncertainties are scaled by a factor $1/\sqrt{\mathcal{L}}$. We combine the chains to form isocontours of 1σ, 2σ, and 3σ significance via their respective p values.

For illustration, we plot these contours in the plane of $A_{\rm FB}^{\rm tot}$ and $\sigma(t\bar{t})$ in Fig. 2(a). We note that the current average values of $A_{\rm FB}$ and $\sigma(t\bar{t})$ are consistent with the SM within the 2σ level. With an upgraded integrated luminosity of $\int \mathcal{L}dt = 10$ fb^{-1} at the Tevatron, the statistical uncer-

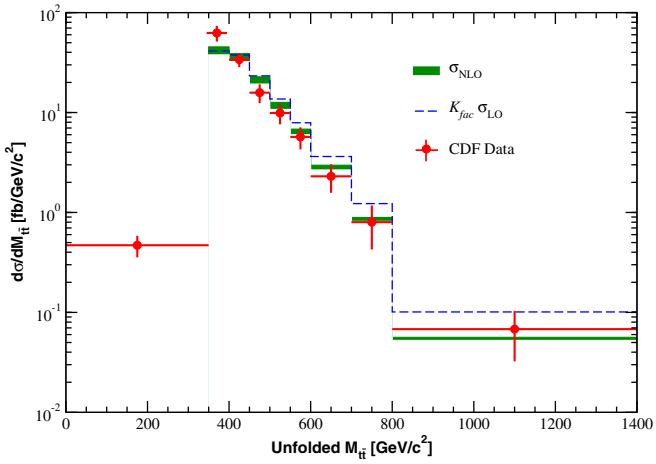

FIG. 1 (color online). The invariant mass spectrum measured by CDF assuming $m_t = 175$ GeV. The solid histogram is the CDF expectation taken from a LO calculation and PYTHIA. The solid band indicates the full NLO SM prediction with a theoretical error due to scale uncertainty which we use in our scans. The dashed line is $K(d\sigma_{\rm LO}/dM_{t\bar{t}})$ with $K = \sigma_{\rm NLO}/\sigma_{\rm LO}$ which shows a large deviation from the data. The data are taken from Ref. [30].

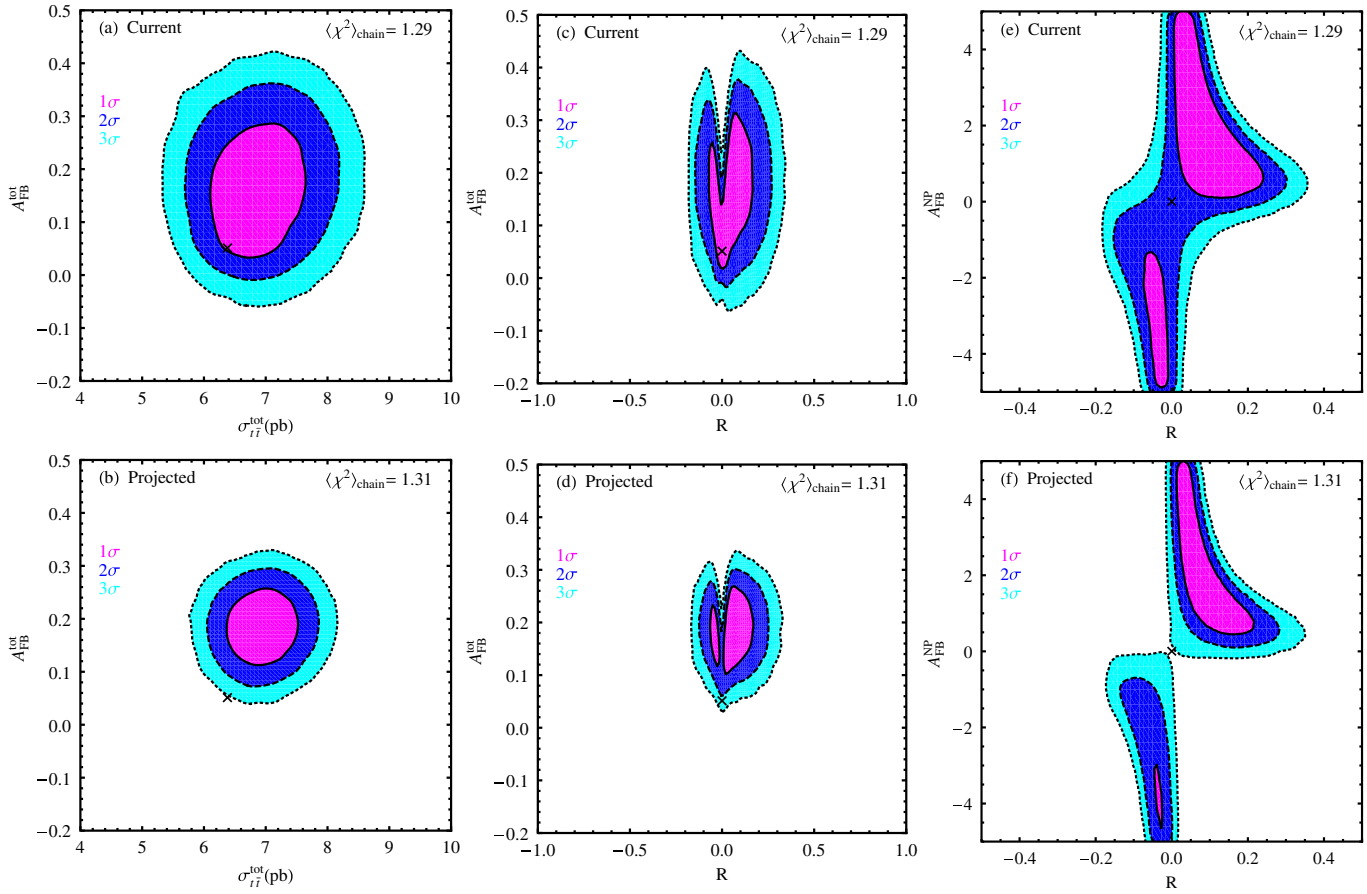

FIG. 2 (color online). (a) Correlation between observed $A_{\rm FB}^{\rm tot}$ and $\sigma(t\bar{t})$ at the Tevatron with the current integrated luminosities; (b) same for $\int \mathcal{L}dt = 10$ fb^{-1}. (c) Correlation between observed $A_{\rm FB}^{\rm tot}$ and fraction of NP contribution to $\sigma(t\bar{t})$ for the current integrated luminosities; (d) same for $\int \mathcal{L}dt = 10$ fb^{-1}. (e) Correlation between the NP-generated asymmetry $A_{\rm FB}^{\rm NP}$ and R for the current integrated luminosities; (f) same for $\int \mathcal{L}dt = 10$ fb^{-1}. Here, we do not include the $M_{t\bar{t}}$ spectrum constraint. In each case the predicted correlations for $\int \mathcal{L}dt = 10$ fb^{-1} assume the same central values of experimental data. The crosses correspond to the standard model predictions of the $A_{\rm FB}$ and $\sigma_{t\bar{t}}$. Innermost contours correspond to 1σ deviation from minimum-χ^2 solutions; next-to-innermost correspond to 2σ; outermost correspond to 3σ. Note that these scans are performed by comparing only to the measurements of the total cross section and asymmetry and not the $M_{t\bar{t}}$ distribution. These should be compared to a SM scan only subject to these two measurements which gives $\langle\chi^2\rangle_{\rm chain} = 2.56$ for the current luminosity and $\langle\chi^2\rangle_{\rm chain} = 6.20$ for 10 fb^{-1} if the central values are unchanged.

tainty would be reduced significantly; see Fig. 2(b). The deviation of $A_{\rm FB}$ from zero is then larger than 3σ. Note that we also allow negative values of $A_{\rm FB}^{\rm tot}$ in this work, though they are not preferred. Taking the SM theory prediction, we translate $\sigma(t\bar{t})$ into R defined in Eq. (6). The correlation of $A_{\rm FB}^{\rm tot}$ and R is shown in Figs. 2(c) and 2(d). Finally, using Eq. (5), we obtain the correlation between $A_{\rm FB}^{\rm NP}$ and R shown in Figs. 2(e) and 2(f). Clearly, the smaller R, the larger $A_{\rm FB}^{\rm NP}$; see the 1σ contour (solid black).

Note that since the MCMC is sensitive to the relative likelihood change in going between two points, it is sensitive to only the $\Delta\chi^2$ values. Therefore, the isocontours of the p values for 1, 2, and 3σ assume the given model. To obtain an overall indication of how well the model in question fits the data, we quote $\langle\chi^2\rangle_{\rm chain}$, the χ^2 per degree of freedom values averaged over the entire chain. In cases where we include the $\frac{d\sigma}{dM_{t\bar{t}}}|_{\rm bin}$ constraint, $N_{\rm dof} = 3$, otherwise $N_{\rm dof} = 2$. This quantity is an overall estimate of the model's consistency with the data. Generally, values of $\langle\chi^2\rangle_{\rm chain} < 2$ are considered fairly good fits, while values much beyond that are not considered very good.

One might be tempted to search for the parameter set that yields the best fit to the given data. However, this is doing so without regard to the level of fine-tuning required to find such a point. Explicitly, this can be seen as a set of points in parameter space by which the χ^2 value is minimized, ideally to zero. However, if a small deviation from these points provides a large increase in χ^2, this particular set of points that provide a good fit can be seen as more fine-tuned compared with another solution set without such a steep increase in χ^2. Therefore, the MCMC approach does take into account the parameter space available that affords a good fit, preferentially solutions with low fine-tuning.

To compare the MCMC results of Fig. 2 and subsequent Figures, we ran a MCMC with a pure SM explanation by explicitly setting $A_{\rm FB}^{\rm NP}$ and $\sigma_{t\bar{t}}^{\rm NP}$ to zero and scanning over Eq. (12) with Gaussian priors. We find that

$$\langle \chi^2 \rangle_{\rm chain}^{\rm SM} = \begin{cases} 2.56 & \text{Current luminosity} \\ 6.20 & \text{Projected: } \int \mathcal{L} dt = 10\ \text{fb}^{-1}, \end{cases} \quad (15)$$

where "Current luminosity" refers to the measurement of $\sigma_{t\bar{t}}$ with an integrated luminosity of 4.6 fb^{-1} and the measurement of $A_{\rm FB}$ with an integrated luminosity of 3.2 fb^{-1}. For the projected integrated luminosity of 10 fb^{-1}, we assume the central values of $A_{\rm FB}^{\rm tot}$ and $\sigma_{t\bar{t}}^{\rm tot}$ remain unchanged from the values taken in Eqs. (2) and (9) while the uncertainties reduce by a scale factor $\sqrt{\mathcal{L}}$. When we examine specific models that could give rise to a larger $A_{\rm FB}$ than the SM, we must also take into account the $M_{t\bar{t}}$ distribution measurement. To compare these models against the SM, we again run a MCMC with a pure SM explanation scanning over $A_{\rm FB}$ and $\sigma_{t\bar{t}}$ as above while also scanning over our NLO prediction (seen in Fig. 1) with Gaussian priors for the last seven bins of the CDF $M_{t\bar{t}}$ distribution. The bin nearest $t\bar{t}$ threshold accounts for the majority of the total cross section. Since we already include the total cross section in our fit, we do not include this bin in our fit of the $M_{t\bar{t}}$ distribution so that we do not weight the total cross section too heavily. If we include the measurement of the $M_{t\bar{t}}$ distribution and perform a MCMC scan over the SM, we find

$$\langle \chi^2 \rangle_{\rm chain}^{\rm SM} = \begin{cases} 1.75 & \text{Current luminosity} \\ 4.22 & \text{Projected: } \int \mathcal{L} dt = 10\ \text{fb}^{-1}. \end{cases} \quad (16)$$

Here, Current luminosity refers to the above values of integrated luminosity for the $\sigma_{t\bar{t}}$ and $A_{\rm FB}$ measurements and 2.7 fb^{-1} for the measurement of the $M_{t\bar{t}}$ distribution. For the projected luminosity of 10 fb^{-1}, we again assume that the central values of all measurements remain the same while their errors scale as $1/\sqrt{\mathcal{L}}$. We note that the values of $\langle \chi^2 \rangle_{\rm chain}$ in Eq. (16) are less than those in Eq. (15). This is because $\langle \chi^2 \rangle_{\rm chain}$ is a χ^2 per degree of freedom. There are two degrees of freedom in Eq. (15) and three in Eq. (16) with the addition of the $M_{t\bar{t}}$ distribution. The good agreement of the $M_{t\bar{t}}$ distribution in the SM with data (seen in Fig. 1) causes the χ^2 per degree of freedom to decrease when it is included in the fit. When comparing models, we can say that if the $\langle \chi^2 \rangle_{\rm chain}$ value for a given model is less than that for the SM with the appropriate data into account, the model will provide a better overall fit to the data than the SM.

The F-B asymmetry, defined in terms of a ratio of cross sections, is very sensitive to the renormalization and factorization scales, μ_R and μ_F, respectively, at which the cross sections are evaluated. The uncertainties in the cross section associated with those scales can be considered as an estimate of the size of unknown higher order contributions. In this study, we set $\mu_R = \mu_F = \mu_0$ and vary it around the central value of $\mu_0 = m_t$, where m_t is the mass of the top quark. Typically, a factor of 2 is used as a rule of thumb. Large scale dependence in the LO cross section can be significantly improved by including the higher order QCD and electroweak corrections. In this work we calculate the SM top pair production cross section with the NLO QCD corrections. Unfortunately, the QCD corrections to the G' induced top pair production are not available yet. Therefore, we calculate the NP contributions only at LO and rescale them by the $M_{t\bar{t}}$-dependent SM $q\bar{q}$ K factors. Because of the mismatch between the SM and NP cross sections, $A_{\rm FB}$ calculated in this way depends on the choice of scale.

Table I shows the LO and NLO top quark pair production cross sections in the SM at the Tevatron. We present the quark annihilation and gluon fusion processes individually as well as their sum. The CTEQ6.6M [21] and CTEQ6L [32] PDF packages are used in the NLO and LO calculations, respectively. In the last row we also list the K factor, defined as the ratio of NLO and LO cross sections, for three scales.

We argue that the higher order corrections cannot be estimated by a K factor (defined as the ratio of NLO and LO cross sections) because the K factor is very sensitive to the scale. Furthermore, the gluon fusion channel contributes much more at the NLO (roughly about $13 \sim 15\%$ of total cross section) than at the LO (only about 5%). Hence, one also needs to take account of the gluon fusion channel contribution when calculating $A_{\rm FB}$.

Another uncertainty originates from the top quark mass. In Table II we show the top pair production cross section for various top quark masses and three scales. The central values of NLO theory calculations for the three masses $m_t = 171.0$ 172.5175.0 GeV are always $\mathcal{O}(1\sigma)$ below the recent CDF results given in Eqs. (7) and (8), suggesting that the NP should contribute positively to $t\bar{t}$ production.

In the following sections, we study a few interesting new physics models which can generate a significant deviation from the SM expectation for $A_{\rm FB}$ in the top quark pair production channel. We also comment on the scale depen-

TABLE I. Predicted LO and NLO top pair production cross sections (pb) in the SM at the Tevatron, with $\mu_0 = m_t = 175$ GeV. Note that the negative $\sigma(gq)$ and $\sigma(g\bar{q})$ cross sections are due to the subtraction to avoid double counting at NLO [21].

	LO			NLO		
	$\mu_0/2$	μ_0	$2\mu_0$	$\mu_0/2$	μ_0	$2\mu_0$
$\sigma(\bar{q}q)$	6.82	5.01	3.79	5.70	5.56	5.04
$\sigma(gg)$	0.37	0.24	0.17	1.00	0.90	0.74
$\sigma(gq)$	0.00	0.00	0.00	0.01	−0.03	−0.05
$\sigma(g\bar{q})$	0.00	0.00	0.00	0.01	−0.03	−0.05
$\sigma_{\rm tot}$	7.19	5.26	3.96	6.72	6.39	5.69
$\sigma_{(gg)}/\sigma_{\rm tot}$	0.05	0.05	0.04	0.15	0.14	0.13
$K_{\rm fac}$				0.93	1.22	1.42

TABLE II. Predicted LO and NLO $t\bar{t}$ production cross sections (pb) for various top quark masses and three scales ($\mu_0/2$, μ_0, $2\mu_0$ with $\mu_0 = m_t$) at the Tevatron.

	LO			NLO		
m_t(GeV)	$\mu_0/2$	μ_0	$2\mu_0$	$\mu_0/2$	μ_0	$2\mu_0$
171.0	8.08	5.91	4.45	7.61	7.23	6.44
172.0	7.84	5.74	4.32	7.37	7.01	6.24
172.5	7.72	5.66	4.26	7.25	6.90	6.14
173.0	7.61	5.57	4.19	7.14	6.79	6.05
174.0	7.40	5.42	4.07	6.92	6.58	5.86
175.0	7.19	5.26	3.96	6.72	6.39	5.69
176.0	6.98	5.11	3.84	6.51	6.19	5.51
177.0	6.78	4.96	3.73	6.31	6.01	5.35

dence in each new physics model. Without losing generality, in the rest of this paper, we set $m_t = 175$ GeV.

III. EXOTIC GLUON

We begin with an exotic gluon (G') model, as the other models can be easily derived from the G' model result. In Sec. III A, we present analytic formulae for $\sigma_{t\bar{t}}$ and $A_{\rm FB}$. We calculate its width in Sec. III B. In Secs. III C, III D, and III E we perform MCMC scans over parameters in several G' scenarios subject to the experimental constraints.

A. Differential cross section and asymmetry

The G' boson couples to the SM quarks also via the QCD strong interaction,

$$G'q\bar{q}\text{: } ig_s t^A \gamma^\mu (f_L P_L + f_R P_R), \tag{17}$$

$$G't\bar{t}\text{: } ig_s t^A \gamma^\mu (g_L P_L + g_R P_R), \tag{18}$$

where we normalize the interaction to the QCD coupling, g_s, and use q to denote light quarks of the first two generations. Such an exotic gluon can originate from an extra-dimensional model such as the Randall-Sundrum model [7], chiral color model [33–42], or top composite model [43]. As discussed below, the axial coupling of G' to the SM quarks is necessary to create a forward-backward asymmetry. In the extra-dimensional model, such nonvector coupling of Kaluza-Klein gluons to fermions arises from localizing the left- and right-handed fermions at different locations in the extra dimension.

The differential cross section with respect to the cosine of the top quark polar angle θ in the $t\bar{t}$ c.m. frame is

$$\frac{d\hat{\sigma}(G')}{d\cos\theta} = \mathcal{A}_{\rm SM} + \mathcal{A}^{G'}_{\rm INT} + \mathcal{A}^{G'}_{\rm NPS}, \tag{19}$$

where

$$\mathcal{A}_{\rm SM} = \frac{\pi\beta\alpha_s^2}{9\hat{s}}(2 - \beta^2 + (\beta\cos\theta)^2), \tag{20}$$

$$\mathcal{A}^{G'}_{\rm INT} = \frac{\pi\beta\alpha_s^2}{18\hat{s}} \frac{\hat{s}(\hat{s} - m^2_{G'})}{(\hat{s} - m^2_{G'})^2 + m^2_{G'}\Gamma^2_{G'}}(f_L + f_R)(g_L + g_R) \times \left\{(2 - \beta^2) + 2\frac{(f_L - f_R)(g_L - g_R)}{(f_L + f_R)(g_L + g_R)}\beta\cos\theta + (\beta\cos\theta)^2\right\}, \tag{21}$$

$$\mathcal{A}^{G'}_{\rm NPS} = \frac{\pi\beta\alpha_s^2}{36\hat{s}} \frac{\hat{s}^2}{(\hat{s} - m^2_{G'})^2 + m^2_{G'}\Gamma^2_{G'}}(f_L^2 + f_R^2)(g_L^2 + g_R^2) \times \left\{1 + \frac{2g_L g_R}{g_L^2 + g_R^2}(1 - \beta^2) + 2\frac{(f_L^2 - f_R^2)(g_L^2 - g_R^2)}{(f_L^2 + f_R^2)(g_L^2 + g_R^2)} \times \beta\cos\theta + (\beta\cos\theta)^2\right\}. \tag{22}$$

Here, the angle θ is defined as the angle between the direction of motion of the top quark and the direction of motion of the incoming quark (e.g., the u quark) in the $t\bar{t}$ c.m. system. The subscripts "SM,", "INT," and "NPS" denote the contribution from the SM, the interference between the SM and NP, and the NP amplitude squared. For the G' model, the SM contribution is from the gluon-mediated s-channel diagram, the NPS contribution from the exotic gluon G'-mediated diagram, and the INT contribution from the interference between the two. The squared c.m. energy of the $t\bar{t}$ system is $\hat{s} = (p_q + p_{\bar{q}})^2$, and $\beta = \sqrt{1 - 4m_t^2/\hat{s}}$ is the top quark velocity in the $t\bar{t}$ c.m. system.

The forward-backward asymmetry of the top quark in the $t\bar{t}$ c.m. frame is defined as

$$A^{t\bar{t}}_{\rm FB} = \frac{\sigma_F - \sigma_B}{\sigma_F + \sigma_B}, \tag{23}$$

where

$$\sigma_F \equiv \int_0^1 \frac{d\sigma}{d\cos\theta} d\cos\theta, \qquad \sigma_B \equiv \int_{-1}^0 \frac{d\sigma}{d\cos\theta} d\cos\theta. \tag{24}$$

We further parameterize the differential cross section $d\sigma/d\cos\theta$ as follows:

$$\frac{d\sigma_i}{d\cos\theta} = A_i + B_i\cos\theta + C_i\cos^2\theta, \tag{25}$$

where the subindex i denotes SM, INT and NPS. Hence, after integrating over the angle θ, we obtain the asymmetry and total cross section

$$A_{\rm FB} = \frac{\sum_i B_i}{\sum_i (2A_i + \frac{2}{3}C_i)}, \quad \text{and} \quad \sigma_{\rm tot} = \sum_i \left(2A_i + \frac{2C_i}{3}\right), \tag{26}$$

where the sums are over the SM, INT, and NPS terms. In reality the incoming quark could originate from either a

proton or an antiproton, but it predominantly comes from a proton due to large valence quark parton distribution functions. Taking the quark from the antiproton and the antiquark from the proton contributes less than 1% of the total $t\bar{t}$ cross section. Therefore, in $\bar{p}p$ collisions at the Tevatron one can choose the direction of the proton to define the forward direction.

Now let us comment on a few interesting features of the asymmetry and cross section generated by the INT and NPS effects individually, because both effects are sensitive to different new physics scales: the former to a higher NP scale and the latter to a lower scale. First, we note that the asymmetry is sensitive to the ratio of coupling (squared) differences and sums for the INT (NPS) effects, e.g.,

$$A_{\rm FB}^{\rm INT} \propto \frac{(f_L - f_R)(g_L - g_R)}{(f_L + f_R)(g_L + g_R)} \times \frac{2\langle\beta\rangle}{2(2 - \langle\beta^2\rangle) + \frac{2}{3}\langle\beta^2\rangle}, \tag{27}$$

$$A_{\rm FB}^{\rm NPS} \propto \frac{(f_L^2 - f_R^2)(g_L^2 - g_R^2)}{(f_L^2 + f_R^2)(g_L^2 + g_R^2)} \times \frac{2\langle\beta\rangle}{2[1 + (1 - \langle\beta^2\rangle)(2g_L g_R)/(g_L^2 + g_R^2)] + \frac{2}{3}\langle\beta^2\rangle}, \tag{28}$$

where $\langle\beta\rangle$ and $\langle\beta^2\rangle$ denote the averaged β and β^2 after integration over the angle θ and convolution of the partonic cross section with parton distribution functions.

To make the physics source of the asymmetry more transparent, we define the reduced asymmetry ($\hat{A}_{\rm FB}$) and reduced cross section $\hat{\sigma}$ as follows:

$$\hat{A}_{\rm FB}^{\rm INT} = A_{\rm FB}^{\rm INT} \Big/ \frac{(f_L - f_R)(g_L - g_R)}{(f_L + f_R)(g_L + g_R)}, \tag{29}$$

$$\hat{A}_{\rm FB}^{\rm NPS} = A_{\rm FB}^{\rm NPS} \Big/ \frac{(f_L^2 - f_R^2)(g_L^2 - g_R^2)}{(f_L^2 + f_R^2)(g_L^2 + g_R^2)}, \tag{30}$$

$$\hat{\sigma}^{\rm INT} = \frac{\sigma^{\rm INT}}{(f_L + f_R)(g_L + g_R)} \tag{31}$$

$$\hat{\sigma}^{\rm NPS} = \frac{\sigma^{\rm NPS}}{(f_L^2 + f_R^2)(g_L^2 + g_R^2)}. \tag{32}$$

The reduced asymmetries and cross sections are easily computed universal functions that allow us to focus on two separate limiting cases; the new physics contribution to $\sigma_{t\bar{t}}$ and $A_{\rm FB}$ is primarily from the INT term if it is produced by a heavy resonance that interferes with the SM production process. If the new physics is due to a resonance that does not interfere with the SM production, then the new contribution to $\sigma_{t\bar{t}}$ and $A_{\rm FB}$ is given by the NPS term. One simply has to multiply the reduced asymmetry or cross section by the appropriate combination of couplings to obtain the full new physics contribution to $\sigma_{t\bar{t}}$ and $A_{\rm FB}$. In Fig. 3, we plot the reduced asymmetry (a) and the reduced cross section (b) as functions of $m_{G'}$ for various choice of $\Gamma_{G'}/m_{G'}$. The reduced asymmetry generated by the INT effects increases rapidly with increasing $m_{G'}$ and finally reaches its maximal value ~0.4. The reduced asymmetry generated by the NPS effects is large, typically around 0.6–0.7. As expected, the reduced cross section of the NPS effects is always positive; cf. the upper three curves in Fig. 3(b). On the other hand, the reduced cross section of the INT effects is always negative due to $(\hat{s} - m_{G'}^2)$ in the numerator of Eq. (20). Both reduced cross sections, especially the NPS effects, are sensitive to the G' decay width. They both go to zero when G' decouples.

The difference between the two reduced asymmetries can be easily understood from the β distribution shown in Fig. 4. Figure 4(a) shows the normalized differential cross section with respect to β for 175 GeV top quark production in the SM at the Tevatron, which peaks around $\beta \sim 0.65$. The INT effects only slightly shift the peak position. Substituting $\langle\beta\rangle \sim 0.65$ into Eqs. (27) and (29), we obtain $A_{\rm FB}^{\rm INT} \simeq 0.4$. On the contrary, the NPS effects prefer a much

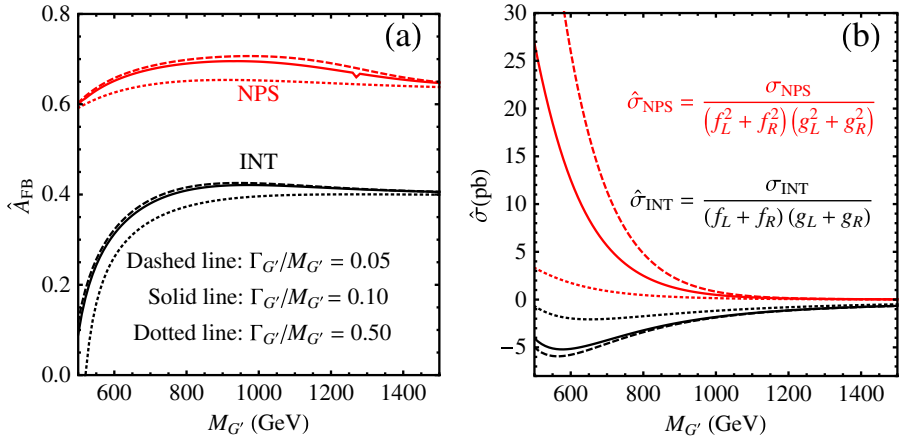

FIG. 3 (color online). (a) Reduced asymmetries defined in Eqs. (29) and (30): $\hat{A}_{\rm FB}^{\rm INT}$ (lower three curves) and $\hat{A}_{\rm FB}^{\rm NPS}$ (upper three curves); (b) Reduced cross sections defined in Eqs. (31) and (32): $\hat{\sigma}^{\rm INT}$ (lower three curves) and $\hat{\sigma}^{\rm NPS}$ (upper three curves).

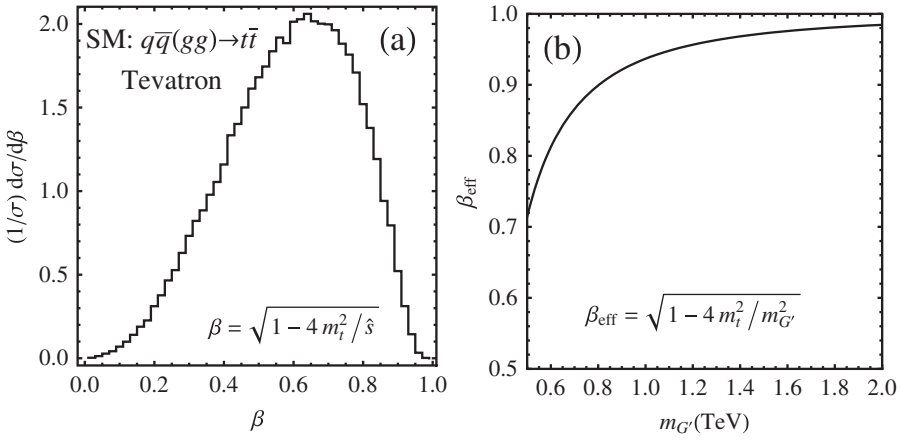

FIG. 4. (a) Normalized differential cross section for $t\bar{t}$ production as a function of $\beta = \sqrt{1-4m_t^2/\hat{s}}$ of a 175 GeV top quark at the Tevatron; (b) $\beta_{\rm eff} = \sqrt{1-4m_t^2/m_{G'}^2}$ as a function of heavy resonance G' mass.

larger β enforced by the heavy G' resonance. We plot $\beta_{\rm eff} = \sqrt{1-4m_t^2/m_{G'}^2}$ in Fig. 4(b), where $\beta_{\rm eff} \sim 0.98$ for a 2 TeV G'. Such a large $\beta_{\rm eff}$ leads to the large value of $\hat{A}_{\rm FB}^{\rm NPS}$ in Fig. 3. For an extremely heavy G', $\beta_{\rm eff}$ is equal to 1, yielding the well-known maximal $\hat{A}_{\rm FB}^{\rm NPS} = 3/4$. When both INT and NPS effects contribute, one cannot factorize out the couplings as in Eqs. (27)–(32) due to the presence of both linear and quadratic coupling terms.

B. G' decay width

The $\mathcal{A}_{\rm NPS}$ term contributes significantly in the vicinity of $m_{G'}$ where the decay width $\Gamma_{G'}$ plays an important role. Hence, it is very important to use an accurate decay width in the parameter scan. We consider the case that the G' boson decays entirely into SM quark pairs, yielding the following partial decay width [41]:

$$\Gamma(G' \to t\bar{t}) = \frac{\alpha_s}{12} m_{G'} \left[(g_L^2 + g_R^2)\left(1 - \frac{m_t^2}{m_{G'}^2}\right) + 6 g_L g_R \frac{m_t^2}{m_{G'}^2} \right], \tag{33}$$

$$\Gamma(G' \to b\bar{b}) = \frac{\alpha_s}{12}(g_L^2 + g_R^2) m_{G'}, \tag{34}$$

$$\Gamma(G' \to \sum q\bar{q}) = N_f \frac{\alpha_s}{12}(f_L^2 + f_R^2) m_{G'}, \tag{35}$$

where $N_f = 4$ denotes the light quark flavors, and we have assumed that b_R couples to G' with the same strength as t_R. In the limit of $M_{G'} \gg m_t$, the total decay width of G' is

$$\Gamma_{G'} = \frac{\alpha_s}{6} m_{G'}[(g_L^2 + g_R^2) + 2(f_L^2 + f_R^2)]. \tag{36}$$

When the couplings $g_{L/R} \simeq f_{L/R}$ are of order 1, $\Gamma_{G'} \simeq \alpha_s M_{G'} \simeq 0.1 M_{G'}$. When $g_{L/R} \approx f_{L/R} \sim 3$, $\Gamma_{G'} \sim M_{G'}$. In the following parameter scan we vary the couplings of the G' boson in the range of -3 to 3 when all couplings are present but -5 to 5 when only two are nonzero.

C. Left-handed G': $f_R = g_R = 0$

Since there are five independent parameters (four couplings and the G' boson mass) in Eqs. (19)–(22), we turn off the right-handed couplings f_R and g_R in order to make the physics origin of the asymmetry more transparent. We first consider $m_{G'} = 1000$ GeV in Sec. III C 1 and then $m_{G'} = 2000$ GeV in Sec. III C 2. We will comment on nonzero f_R and g_R in Secs. III D and III E.

1. $m_{G'} = 1000$ GeV

We first examine theoretical predictions of $A_{\rm FB}^{\rm tot}$ and $\sigma_{\rm INT}$ and $\sigma_{\rm NPS}$ before we perform a MCMC scan over the parameters. By "theoretical" we mean that the asymmetry and the top pair production cross section are calculated independently, without regard to their correlation. Figure 5(a) displays the cross section contours generated by the INT effects ($\sigma_{\rm INT}$). The INT effects could be either positive or negative, depending on the sign of the coupling product $f_L g_L$. The INT effects dominate in the region of $\sqrt{\hat{s}} < m_{G'}$, so their contribution to the top pair production cross section can be written as

$$\sigma_{\rm INT} \propto -(m_{G'}^2 - \hat{s}) f_L g_L. \tag{37}$$

This expression thus yields a positive contribution to the cross section when $f_L g_L < 0$ (i.e., the second and fourth quadrants in Fig. 5) and a negative contribution when $f_L g_L > 0$ (i.e., the first and third quadrants).

On the contrary, the NPS contribution is always positive; see Fig. 5(b). Since the NPS effects contribute mainly in the vicinity of $m_{G'}$, i.e., $\hat{s} \simeq m_{G'}^2$, their contribution to the top pair production cross section can be written as follows:

$$\sigma_{\rm NPS} \propto \frac{f_L^2 g_L^2}{\Gamma_{G'}^2} \sim \frac{f_L^2 g_L^2}{m_{G'}^2 (2f_L^2 + g_L^2)^2}. \tag{38}$$

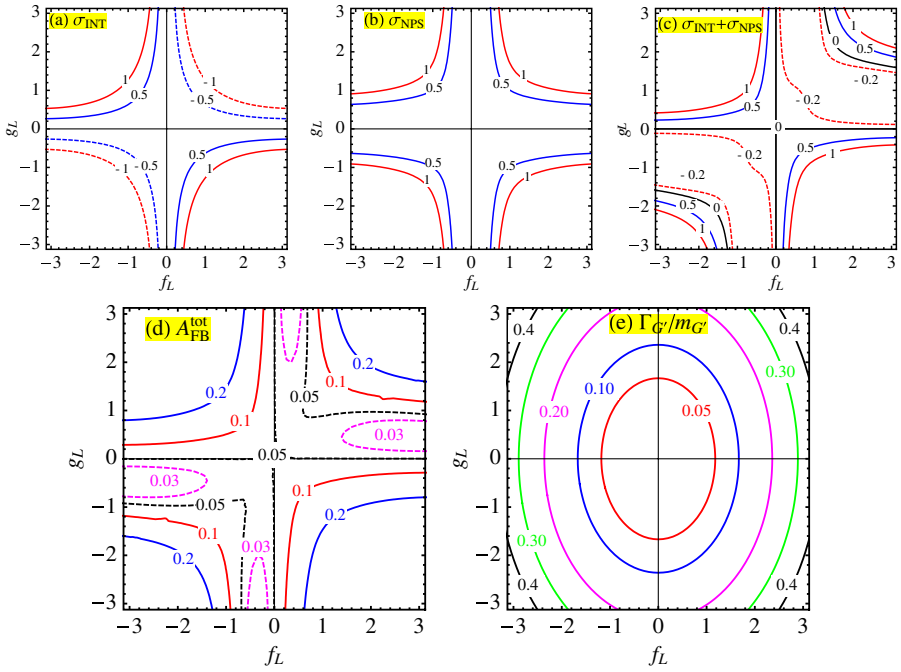

FIG. 5 (color online). Theoretical prediction contours in the plane of f_L and g_L with $f_R = g_R = 0$ for a 1 TeV G': (a) contours of cross section (pb) induced by the INT effects, (b) contours of cross section induced by the NPS effects, (c) contours of net cross section of the INT and NPS effects, (d) contours of the observed asymmetry, (e) contours of $\Gamma_{G'}/m_{G'}$.

Hence, the contour pattern of $\sigma_{\rm NPS}$ is determined by $f_L^2 g_L^2/(2f_L^2 + g_L^2)^2$. Figure 5(c) shows the competition between the INT and NPS effects. For a 1 TeV G', the INT generally dominates over the NPS. Note that the contours of net cross section are not symmetric between f_L and g_L due to the width effects. In Fig. 5(d), we see that, except for small couplings in the upper-right and lower-left quadrants, a positive asymmetry can be generated in all four quadrants. In the upper-right and lower-left quadrants, for $|f_L|, |g_L| \gtrsim 3$, the NPS term is large enough to generate a positive $A_{\rm FB}$. Note that negative values of $A_{\rm FB}$, although not plotted in Fig. 5(d), are still consistent with the Tevatron data within 3σ C.L. and are included in the following analysis.

Now we perform a MCMC scan over the parameter space after combining measurements of the $t\bar{t}$ asymmetry, the total cross section, and $\frac{d\sigma}{dM_{t\bar{t}}}$. To obtain the $M_{t\bar{t}}$ distribution, we separate the contribution from the $q\bar{q}$ initial state (which includes the NP that we analyze) from that of the gg initial state, noting that the gq and $g\bar{q}$ contributions are negligible as seen in Table I. We multiply these leading order results by the SM K factors, $K_{q\bar{q}}$ and K_{gg}, respectively, which are obtained by using the Monte Carlo program MCFM [44] to calculate the full NLO SM differential cross section. Each K factor itself differs as a function of $M_{t\bar{t}}$ (as seen in [45]) and so we weight each bin in the $M_{t\bar{t}}$ distribution by the appropriate K factors. We vary the scale μ_0 at which we evaluate the NLO differential cross section between $m_t/2$ and $2m_t$, which gives a range of K factors for each $M_{t\bar{t}}$ bin. This is used in our fits as our estimate of the theoretical uncertainty. This uncertainty is about 10% in the first six bins and around 15% in the last bin. Observe that this procedure, when NP effects are decoupled, reproduces the exact NLO SM differential cross section seen in Fig. 1. In this and subsequent Figures of MCMC distributions, we adopt flat priors in all variables scanned. The priors for the SM-only contribution to the $t\bar{t}$ cross section and $A_{\rm FB}$ are given in Eq. (13). Figure 6(a) displays the parameter space consistent with both measurements at the 1σ (innermost region), 2σ (next-to-innermost region) and 3σ (outermost region) level, respectively, for $m_{G'} = 1000$ GeV. Remember, the isocontours of the p values for 1, 2, and 3σ assume the given model, while the $\langle\chi^2\rangle_{\rm chain}$ value gives an indication of the overall fit. In this case, we get a somewhat worse fit to both experimental results than in the SM, with $\langle\chi^2\rangle_{\rm chain} = 1.84$. Figure 6(b) shows the estimated parameter space contours with an integrated luminosity of 10 fb^{-1}, assuming the central values of both experimental measurements are not changed. The quality of the fit is marginally better than in the SM, with $\langle\chi^2\rangle_{\rm chain} = 4.20$ vs 4.22 in the SM. We observe that the regions where f_L or g_L are small provide the best fit. The boundaries of all three contours can be understood from the theoretical predictions in Figs. 5(c) and 5(d). To explain the discrepancy in the total cross section and in the asymmetry, values of f_L and g_L in the top-left or bottom-right quadrants would be preferred. However, couplings here inevitably worsen the $M_{t\bar{t}}$ distribution. In the top-right and bottom-left quadrants the fit to the $M_{t\bar{t}}$ distribution is improved for small couplings ($|f_L|$,

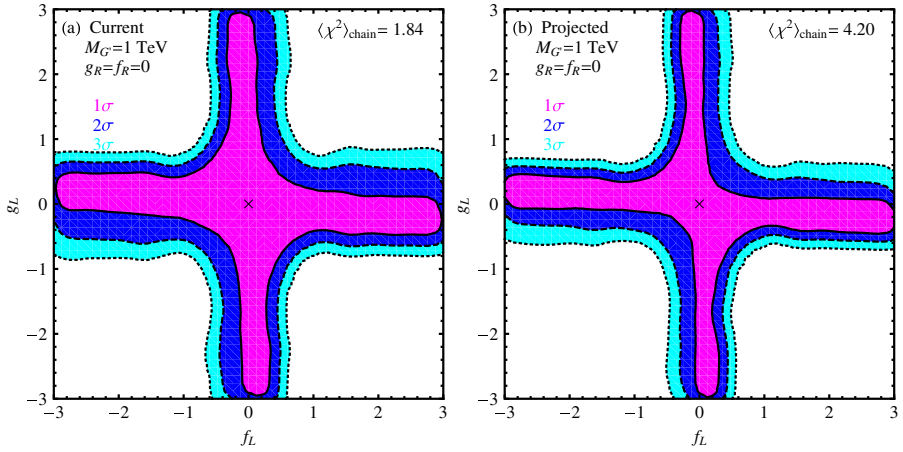

FIG. 6 (color online). Correlation of couplings for $m_{G'} = 1000$ GeV with $f_R = g_R = 0$. Figures on left are for the current integrated luminosity while those on right are for $\int \mathcal{L} dt = 10$ fb^{-1}. The regions inside the contours are preferred, corresponding to 1σ (innermost), 2σ (next-to-innermost), and 3σ (outermost). The crosses correspond to $f_L = g_L = 0$.

$|g_L| \lesssim 1$) but the agreement with the total cross section is slightly worse and an asymmetry smaller than the SM value is generated. For intermediate couplings in these two quadrants ($1 \lesssim |f_L|, |g_L| \lesssim 2$), the fit to the $M_{t\bar{t}}$ distribution is improved but the total cross section is reduced too much and the asymmetry is not improved significantly. Eventually, at large values of the couplings in these quadrants ($|f_L|, |g_L| \gtrsim 2.5$), a large asymmetry is generated and the fit to the total cross section is improved but the $M_{t\bar{t}}$ distribution is greatly worsened. Furthermore, we note that the bands along the $g_L = 0$ axis are slightly wider than those along the $f_L = 0$ axis due to the asymmetric contributions of f_L and g_L to $\Gamma_{G'}$, cf. Fig. 5(e).

2. $m_{G'} = 2000$ GeV

When the G' boson is very heavy, only the interference term in Eq. (21) contributes to $A_{\rm FB}$, leading to

$$A_{\rm FB}^{\rm INT} \propto \frac{(f_L - f_R)(g_L - g_R)}{(f_L + f_R)(g_L + g_R)}. \tag{39}$$

This dependence is illustrated in Fig. 7. In order to get positive corrections to $A_{\rm FB}^{\rm tot}$ and the top pair production cross section, the product $f_L g_L$ needs to be negative to compensate the negative sign from the denominator of the propagator $1/(\hat{s} - m_{G'}^2)$, which is what we see in the upper-left and lower-right quadrants of Figs. 7(a) and 7(b). The results of the MCMC scan are shown in Fig. 8 for $m_{G'} = 2000$ GeV. The contours look quite different from those in Fig. 6. We note that values of f_L and g_L in the upper-left and lower-right quadrants are preferred, which is where a large positive asymmetry is generated as seen in Fig. 7. This shows that the $M_{t\bar{t}}$ distribution is less constraining than in the $m_{G'} = 1$ TeV case as one would expect. The fit to the three experiments gives $\langle\chi^2\rangle_{\rm chain} = 1.69$ for the current integrated luminosity which is slightly better than in the SM where $\langle\chi^2\rangle_{\rm chain} = 1.75$. The fit is improved relative to the SM at the upgraded luminosity with $\langle\chi^2\rangle_{\rm chain} = 3.82$ if the central values do not change as compared to the SM value of $\langle\chi^2\rangle_{\rm chain} = 4.22$.

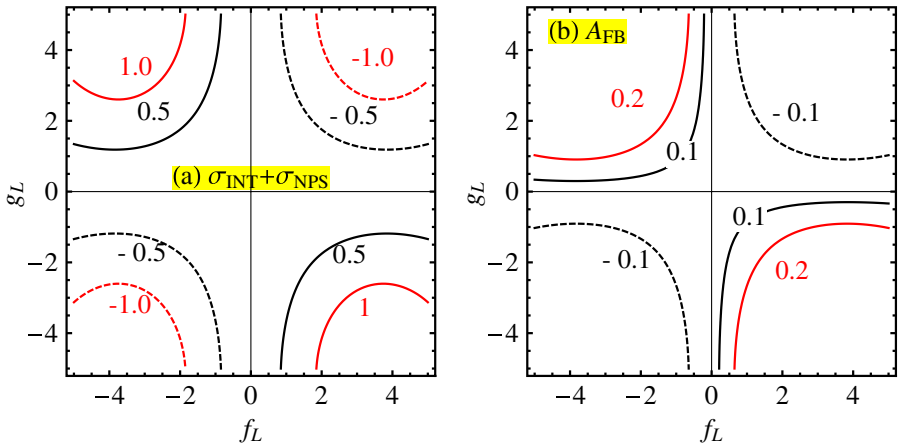

FIG. 7 (color online). Theoretical prediction contours for $m_{G'} = 2000$ GeV with $f_R = g_R = 0$ in the plane of f_L and g_L with $f_R = g_R = 0$: (a) cross section (pb) and (b) $A_{\rm FB}^{\rm tot}$.

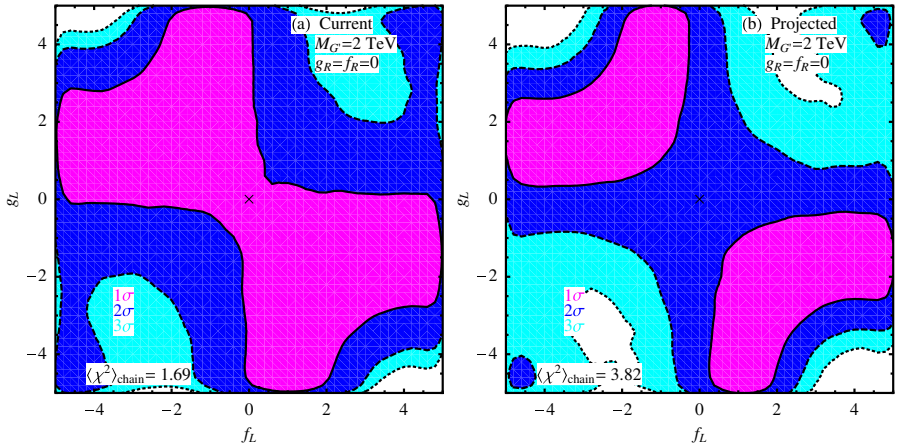

FIG. 8 (color online). Same as Fig. 6 but for $m_{G'} = 2000$ GeV. The region bounded by the solid curve defines the 1σ region, the areas bounded by the dashed lines are within 2σ, and the areas bounded by the dotted lines are within 3σ.

In Fig. 8, we observe that the upper-right and lower-left quadrants are not as tightly constrained as in the $m_{G'} = 1$ TeV case in Fig. 6. Here, the $M_{t\bar{t}}$ distribution is improved.[1] In the case of the 1 TeV G' large couplings in these quadrants decrease the total cross section and asymmetry too much. However, in the 2 TeV case for large couplings in the upper-right and lower-left quadrants the NPS term becomes important due to the large width effects, and this can mitigate the negative contribution to $\sigma_{t\bar{t}}$ and $A_{\rm FB}$ from the INT term allowing for a better fit. This is why the 2 and 3σ regions are not tightly constrained in the upper-right and lower-left quadrants for a 2 TeV G' in Fig. 8. Again, we note that the bands along the f_L and g_L axes are not symmetric due to their asymmetric contributions to $\Gamma_{G'}$.

D. Axigluon: $f_R = -f_L$ and $g_R = -g_L$

Now we study the axigluon case, in which G' only has axial couplings to the quark sector. This type of model has been explicitly proposed as an explanation of the $A_{\rm FB}$ measurement without significantly affecting the total cross section [8,11]. There, the SM prediction for the $t\bar{t}$ cross section was taken to be larger than our value due to differences in m_t and including incomplete NNLO calculations. Therefore, they did not need a significant correction to the cross section.

In the axial limit, only the asymmetry-generating term of the INT in Eq. (22) remains. In general, all terms in the NPS remain. Therefore, at large $m_{G'}$, the INT term dominates and a rather large asymmetry can arise without a sizable contribution to $\sigma_{t\bar{t}}$ or to $\frac{d\sigma}{dM_{t\bar{t}}}$. At lower values of $m_{G'}$, the NPS term is increasingly relevant.

[1]Naively, one might expect that the $M_{t\bar{t}}$ distribution would not be very important for a G' with $m_{G'} = 2$ TeV. However, for couplings f_L, $g_L \sim 4$ the width of the G' can be comparable to $m_{G'}$ (for $f_L = 4$, $g_L = 0$, $\Gamma_{G'} \simeq 0.5 m_{G'}$) and the 2 TeV G' can contribute to the 800 GeV $< M_{t\bar{t}} <$ 1400 GeV bin.

1. $m_{G'} = 1000$ GeV

We show theoretical contours of $\sigma_{\rm NPS}$ (since $\sigma_{\rm INT}$ vanishes when integrated over $\cos\theta$ in the axigluon case) and $A_{\rm FB}^{\rm tot}$ in Fig. 9(a) and 9(b) for an axigluon of mass 1 TeV. We observe that a positive asymmetry is generated when the product fg, with $f = f_L = -f_R$ and $g = g_L = -g_R$, is negative as we expect from Eq. (21). In Fig. 10(a) and 10(b), we perform MCMC scans and find a fit with $\langle\chi^2\rangle_{\rm chain} = 1.56$ for the current luminosity and $\langle\chi^2\rangle_{\rm chain} = 2.94$ for 10 fb^{-1} assuming the central values of the measurements do not change. Small values of either f or g are preferred due to the constraint on the $M_{t\bar{t}}$ distribution. These values of

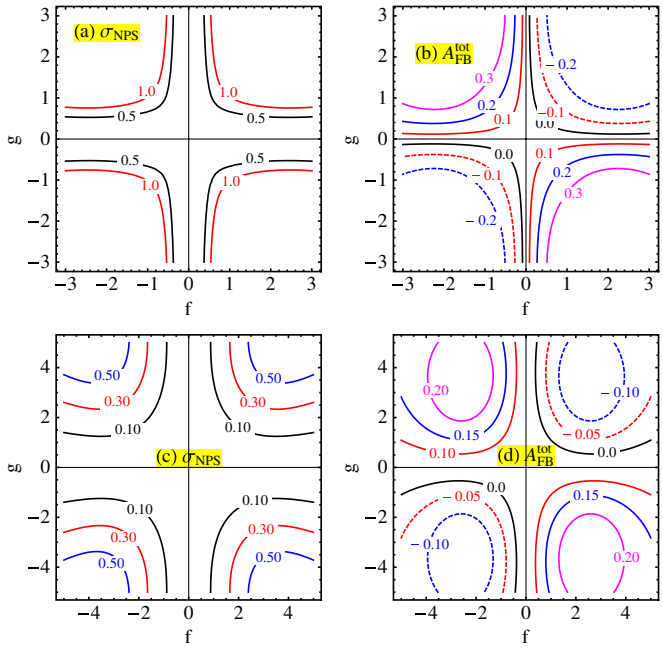

FIG. 9 (color online). Theoretical prediction contours for an axigluon of $\sigma_{\rm NPS} = \sigma_{\rm NP}$ (since $\sigma_{\rm INT} = 0$) and $A_{\rm FB}^{\rm tot}$ for (a,b) $m_{G'} = 1000$ GeV and (c,d) $m_{G'} = 2000$ GeV.

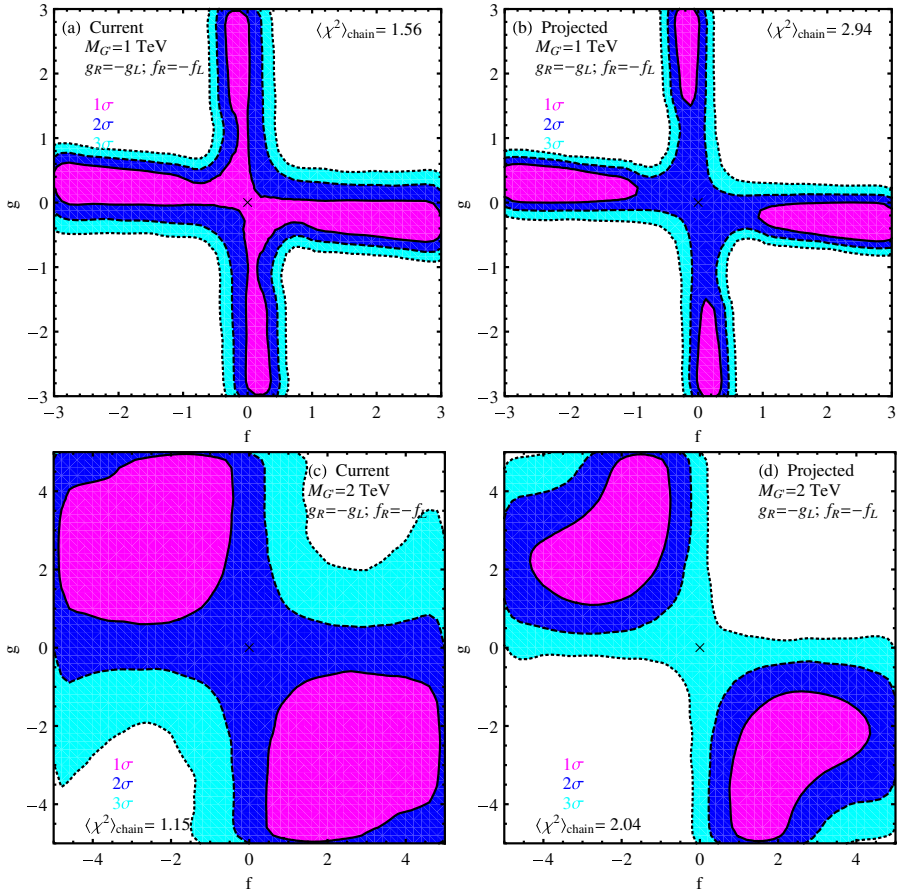

FIG. 10 (color online). Correlation of couplings for $m_{G'} = 1000$ GeV (top panels) and $m_{G'} = 2000$ GeV (bottom panels) in the axigluon limit with the current integrated luminosity (left panels) and $\int \mathcal{L} dt = 10$ fb^{-1} (right panels) assuming the central values of the measurements do not change.

$\langle\chi^2\rangle_{\rm chain}$ for the 1 TeV axigluon are better than the corresponding values in the SM fit. This indicates that a 1 TeV axigluon has less tension with the current data than the SM and would also offer an improvement over the SM if the central values of the data remain the same with an upgraded luminosity of 10 fb^{-1}.

2. $m_{G'} = 2000$ GeV

For a 2 TeV axigluon, we plot theoretical contours of $\sigma_{\rm NPS}$ and $A_{\rm FB}$ in Figs. 9(c) and 9(d). In Figs. 10(c) and 10(d), we show the results of a scan in the case of an axigluon with $m_{G'} = 2000$ GeV. The fit shows better agreement with the data in this case than in the SM, with $\langle\chi^2\rangle_{\rm chain} = 1.15$ for the current luminosity and $\langle\chi^2\rangle_{\rm chain} = 2.04$ for 10 fb^{-1} if the central values do not change. Because of the lessening of the $M_{t\bar{t}}$ constraint for a heavier axigluon, the scans show somewhat different structure than in the 1 TeV case. The 1σ allowed regions are located in the quadrants where $fg < 0$, which is where a positive $A_{\rm FB}$ is generated as seen in Fig. 9(d). The regions of large coupling are constrained by the $M_{t\bar{t}}$ distribution. There is again a slight asymmetry in the width of the allowed regions near the f and g axes due to the asymmetry in the width.

Our results suggest that a heavy axigluon can offer a good explanation of the large $A_{\rm FB}$ observed without increasing the disagreement in the $M_{t\bar{t}}$ distribution too much, as proposed in Ref. [11].

E. Other combinations of couplings

Now let us study different combinations of couplings, e.g., $f_L = g_L = 0$, $f_L = g_R = 0$, and $f_R = g_L = 0$. Figure 11 shows the MCMC scan results of various combinations of couplings with $m_{G'} = 2000$ GeV and with the current luminosity. Purely right-handed couplings in the q-$\bar{q}$-G' interaction give rise to the exactly same result as purely left-handed couplings, cf. Fig. 8(a). But mixed combinations of left-handed and right-handed couplings, e.g., $g_L = f_R = 0$ and $g_R = f_L = 0$, result in a worse fit, with $\langle\chi^2\rangle_{\rm chain} = 1.92$, which is worse than the SM. This is mainly due to the INT effects which are sensitive to the signs of couplings; see Eqs. (21) and (27). Choosing $f_L = g_R = 0$ or $f_R = g_L = 0$ causes the INT effects to generate a negative $A_{\rm FB}^{\rm INT}$, leading to the bad fit.

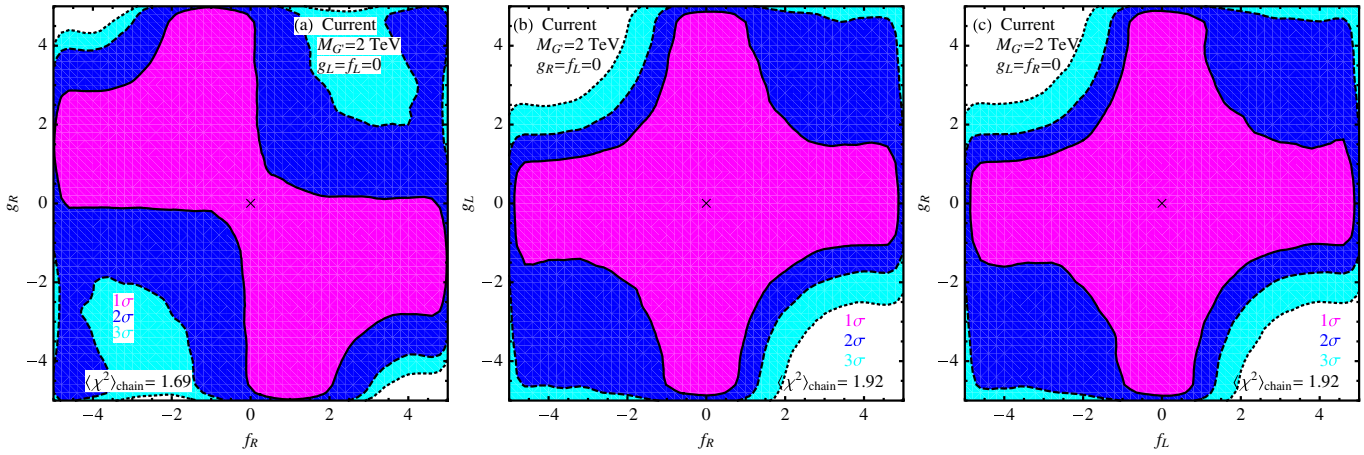

FIG. 11 (color online). Correlation of couplings for $m_{G'} = 2$ TeV with the current integrated luminosity for (a) $g_L = f_L = 0$, (b) $g_R = f_L = 0$, (c) $g_L = f_R = 0$.

IV. EFFECTIVE FIELD THEORY

For a 2 TeV G' boson, due to the broad decay width, the NPS contribution is still sizable for large couplings in the above MCMC scans. It is interesting to ask what the effects are if only the INT term contributes. To that end, in this section we consider dimension-six effective operators that can interfere with the SM top quark pair production channel $q\bar{q} \to g \to t\bar{t}$. We further assume that the scale of the new physics is large enough that the NPS contributions (i.e. $\propto 1/\Lambda^4$ with Λ the new physics scale) can be neglected. For illustration we focus only on the operators which couple left-(right-)handed light quarks to left-(right-) handed top quarks so that contact with Sec. III C can be made. They are listed as follows:

$$\mathcal{O}_{qq}^{(8,1)} = (\bar{q}\gamma_\mu t^A q)(\bar{Q}\gamma^\mu t^A Q), \tag{40}$$

$$\mathcal{O}_{qq}^{(8,3)} = (\bar{q}\gamma_\mu t^A \tau^I q)(\bar{Q}\gamma^\mu t^A \tau^I Q), \tag{41}$$

$$\mathcal{O}_{ut}^{(8,1)} = (\bar{u}\gamma_\mu t^A u)(\bar{t}\gamma^\mu t^A t), \tag{42}$$

$$\mathcal{O}_{dt}^{(8,1)} = (\bar{d}\gamma_\mu t^A d)(\bar{t}\gamma^\mu t^A t), \tag{43}$$

where q and Q denote the $SU(2)_L$ doublets of the light (first two generation) quarks and heavy (third generation) quark, respectively, and $u(d, t)$ are the right-handed gauge singlets. Here, t^A and τ^I are the $SU(3)$ and $SU(2)$ matrices; appropriate contractions are understood. The first index in the superscripts of operators labels the color octet and the second index denotes the weak isospin. Other color and weak singlet operators are omitted as they cannot interfere with the SM channel.

The effective Lagrangian of the four fermion interaction $q\bar{q}t\bar{t}$ is thus given by

$$\mathcal{L}^{(4f)} = g_s^2 \frac{\kappa_L^q}{\Lambda^2}(\bar{q}\gamma_\mu P_L q)(\bar{t}\gamma_\mu P_L t) + g_s \frac{\kappa_R^q}{\Lambda^2}(\bar{q}\gamma_\mu P_R q)(\bar{t}\gamma_\mu P_R t), \tag{44}$$

where we explicitly factor out a strong coupling strength g_s^2, and the reduced coefficients are given as follows:

$$\kappa_L^u = C_{qq}^{(8,1)} + C_{qq}^{(8,3)}, \qquad \kappa_L^d = C_{qq}^{(8,1)} - C_{qq}^{(8,3)},$$
$$\kappa_R^u = C_{ut}^{(8)}, \qquad \kappa_R^d = C_{dt}^{(8)}.$$

Here, the $SU(3)$ generators are omitted, and Λ denotes the new physics scale.

The differential cross section of the effective field theory (EFT) can be easily derived from Eq. (21) by taking the limit of $m_{G'} = \Lambda \gg \sqrt{\hat{s}}$,

$$\mathcal{A}_{\rm INT}^{\rm EFT} = -\frac{\pi\beta\alpha_s^2}{18}\left[\frac{\kappa_L^q + \kappa_R^q}{\Lambda^2}\right] \times \{(2-\beta^2) + 2\beta\cos\theta + (\beta\cos\theta)^2\}. \tag{45}$$

Obviously, the coefficients $\kappa_{L/R}^q$ only affect R but not $A_{\rm FB}^{\rm NP}$. We extract the cutoff scale and coefficients as follows:

$$\mathcal{A}_{\rm INT}^{\rm EFT} = \frac{\kappa_L^q + \kappa_R^q}{(\frac{\Lambda}{\rm TeV})^2} \times \left\{-\frac{\pi\beta\alpha_s^2}{18({\rm TeV})^2}[(2-\beta^2) + 2\beta\cos\theta + (\beta\cos\theta)^2]\right\}, \tag{46}$$

which yields, after integration over $\hat{s}$ and convolution with PDFs,

$$\frac{d\sigma_{\rm EFT}^{\rm INT}}{d\cos\theta} = \frac{\kappa_L^q + \kappa_R^q}{(\frac{\Lambda}{\rm TeV})^2}(A_{\rm EFT} + B_{\rm EFT}\cos\theta + C_{\rm EFT}\cos^2\theta).$$

The parameters $(A_{\rm EFT}, B_{\rm EFT}, C_{\rm EFT})$ are listed in Table III for various choices of factorization scale, where $A_{\rm FB}^{\rm EFT}$ and $\sigma_{\rm EFT}$ are evaluated using Eq. (26). It is clear that one needs

TABLE III. Parameter ($A_{\rm EFT}$, $B_{\rm EFT}$, $C_{\rm EFT}$) for EFT where $A_{\rm FB}^{\rm INT}$ and $\sigma_{\rm EFT}^{\rm INT}$ are calculated after integrating over the angle θ.

$u\bar{u} \to t\bar{t}$						$d\bar{d} \to t\bar{t}$				
μ_R	$A_{\rm EFT}$	$B_{\rm EFT}$	$C_{\rm EFT}$	$A_{\rm FB}^{\rm EFT}$	$\sigma_{\rm EFT}$	$A_{\rm EFT}$	$B_{\rm EFT}$	$C_{\rm EFT}$	$A_{\rm FB}^{\rm EFT}$	$\sigma_{\rm EFT}$
$m_t/2$	−0.294	−0.256	−0.092	0.395	−0.648	−0.052	−0.040	−0.040	0.355	−0.113
m_t	−0.215	−0.185	−0.066	0.392	−0.473	0.037	−0.0288	−0.10	0.353	−0.062
$2m_t$	−0.165	−0.141	−0.050	0.389	−0.363	−0.028	−0.022	−0.007	0.350	−0.082

positive κ_L^q or κ_R^q to get positive $A_{\rm FB}$ but this inevitably gives rise to a negative contribution to $\sigma(t\bar{t})$. Hence, it is difficult to fit both the asymmetry and the top pair production cross section simultaneously at the 1σ level.

Since one cannot separate the coefficient κ from the cutoff Λ, we scan over the combination $\kappa/(\Lambda/\text{TeV})^2$ and limit ourselves to the region of $|\kappa/(\Lambda/\text{TeV})^2| < 10$ in the MCMC scan. In Fig. 12, we plot the correlations between $\kappa/(\Lambda/\text{TeV})^2$ and $\sigma_{\rm tot}$ (top row) and between $\kappa/(\Lambda/\text{TeV})^2$ and $A_{\rm FB}^{\rm tot}$ (bottom row). For the current luminosity, the fit quality of the EFT is worse than the SM, $\langle\chi^2\rangle_{\rm chain} = 1.80$. The fit is marginally better than the SM, $\langle\chi^2\rangle_{\rm chain} = 4.20$, for an integrated luminosity of 10 fb^{-1} if the central values of the measurements remain the same. The fit is worse than that of the 2 TeV left-handed G' due to the lack of a NPS term to balance the contributions of the INT term. This indicates the importance of resonance effects in the fit.

V. FLAVOR-CONSERVING Z' BOSON

An additional Z' can generate a nonzero $A_{\rm FB}$ if its coupling to quarks does not respect parity,

$$Z'q\bar{q}\text{: } ie\gamma^\mu(f_L P_L + f_R P_R), \tag{47}$$

$$Z't\bar{t}\text{: } ie\gamma^\mu(g_L P_L + g_R P_R), \tag{48}$$

where e denotes the electromagnetic coupling strength. In contrast to G', there is no interference between the Z'-mediated top quark pair production and the SM process. Even though the Z' amplitude interferes with the SM

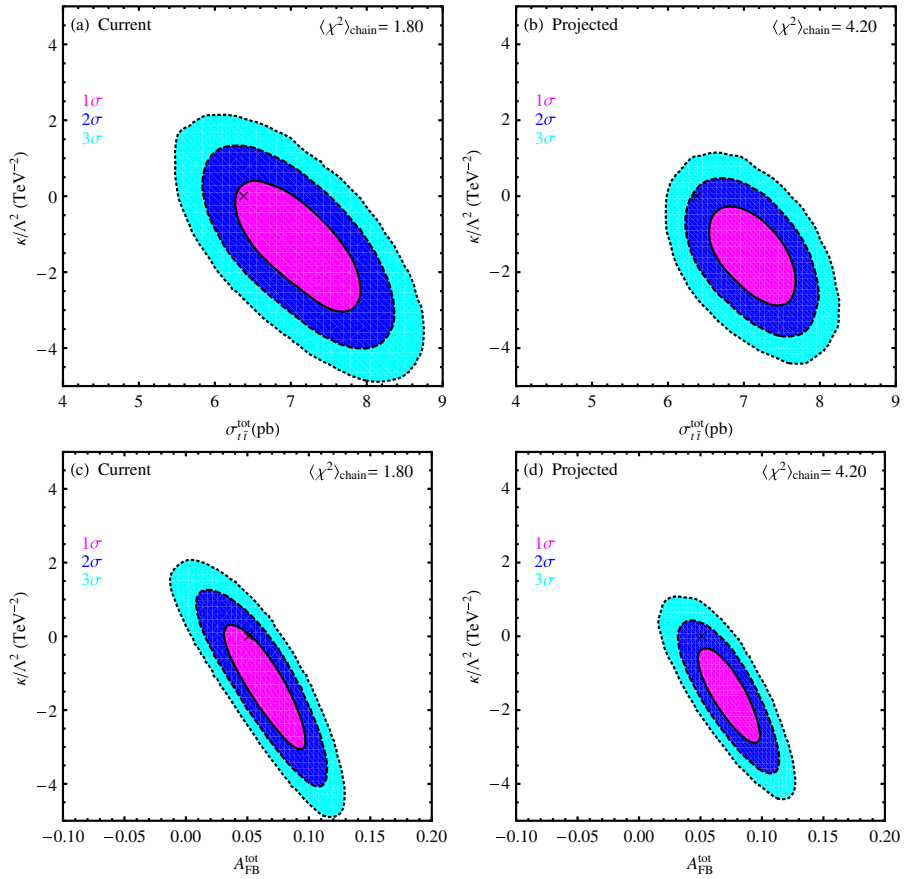

FIG. 12 (color online). (Left): Fitting contours in the EFT with the current integrated luminosity: (a) in the plane of $A_{\rm FB}^{\rm tot}$ and $\kappa/(\Lambda/\text{TeV})^2$, (b) in the plane of $\sigma(t\bar{t})$ and $\kappa/(\Lambda/\text{TeV})^2$. (Right): same as the left column but for $\int \mathcal{L}dt = 10$ fb^{-1}.

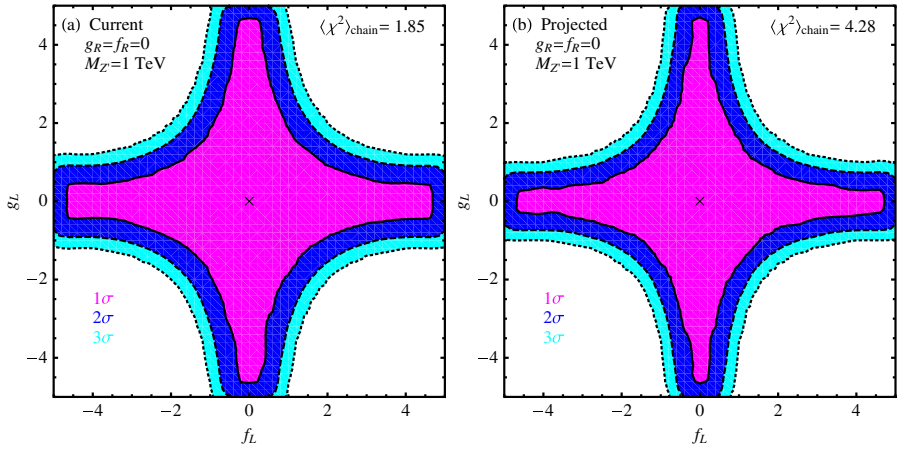

FIG. 13 (color online). Same as Fig. 6 but for 1000 GeV Z'.

process $q\bar{q} \to \gamma^*/Z^* \to t\bar{t}$, the latter contribution is negligible at the Tevatron. Only the NP resonance itself contributes to $A_{\rm FB}$ when the collider energy is large enough to see the resonance effects. We consider the case where both the up and down quarks are gauged, but it is also possible to gauge the up and down quarks differently [46].

Since the interference is absent for the color singlet Z', only $\mathcal{A}_{\rm NPS}$ contributes to NPS. For the s-channel diagram, the differential cross section of Z' can be easily derived from that of G' by omitting the color factor 2/9 in Eq. (21) and replacing α_s by $\alpha_{\rm em}$, yielding

$$\begin{aligned}\frac{d\sigma}{d\cos\theta}\bigg|_{Z'} &= \frac{\pi\beta\alpha_s^2}{9\hat{s}}\frac{9}{2}\mathcal{A}_{\rm NPS}^{G'}\bigg|_{m_G\to m_{Z'},\alpha_s\to\alpha_W} \\ &= \frac{\pi\beta\alpha_{\rm em}^2}{8\hat{s}}\frac{\hat{s}^2}{(\hat{s}-m_G^2)^2+m_G^2\Gamma_G^2}(f_L^2+f_R^2) \\ &\quad\times(g_L^2+g_R^2)\bigg\{1+\frac{2g_Lg_R}{g_L^2+g_R^2}(1-\beta^2) \\ &\quad+2\frac{(f_L^2-f_R^2)(g_L^2-g_R^2)}{(f_L^2+f_R^2)(g_L^2+g_R^2)}\beta\cos\theta+(\beta\cos\theta)^2\bigg\}. \end{aligned} \tag{49}$$

Negative searches for the Z' boson at the Tevatron impose several lower bounds on the Z' mass, roughly above 1 TeV for couplings of order electroweak size. For a leptophobic Z' boson, the bound is slightly looser, $m_{Z'} > 700$ GeV. Owing to the rapid drop of the PDFs, the Z' boson contributes significantly only in the resonance region, where $\beta \to 1$. Further noting that the coefficient of the $(1-\beta^2)$ term in Eq. (49) is always less than one, we can drop this term and obtain

$$A_{\rm FB}^{Z'} \propto \frac{(f_L^2-f_R^2)(g_L^2-g_R^2)}{(f_L^2+f_R^2)(g_L^2+g_R^2)}. \tag{50}$$

As in the G' study, we turn off the right-handed couplings first. Figure 13 displays the correlation between f_L and g_L couplings for a 1000 GeV Z' boson with $f_R = g_R = 0$. Like the 1 TeV G', the $M_{t\bar{t}}$ distribution favors smaller f_L or g_L. The fit is worse than in the SM with $\langle\chi^2\rangle_{\rm chain} = 1.85$ for the current luminosity and $\langle\chi^2\rangle_{\rm chain} = 4.28$ for 10 fb^{-1} if the central values remain the same. For a 2 TeV Z' boson with $f_R = g_R = 0$, we see the results of the MCMC scan in Fig. 14. The fit is somewhat better than the SM: $\langle\chi^2\rangle_{\rm chain} = 1.62$ for the current luminosity and

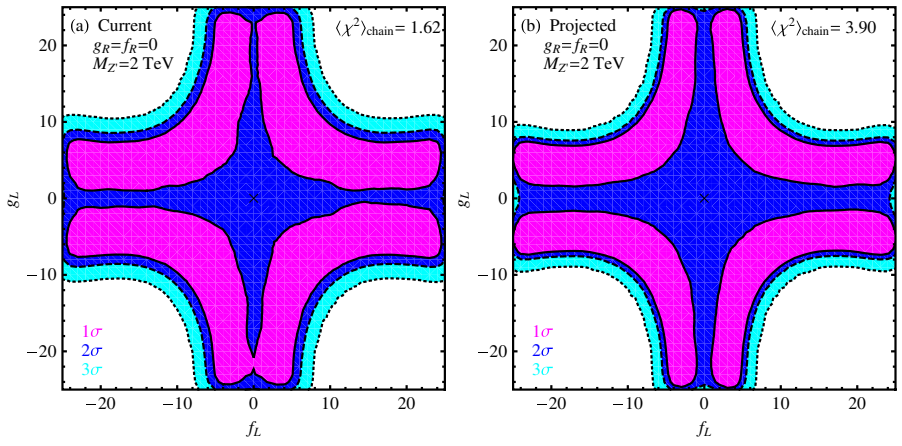

FIG. 14 (color online). Same as Fig. 6 but for 2 TeV Z'.

$\langle\chi^2\rangle_{\text{chain}} = 3.90$ for 10 fb^{-1} due to the lessening of the importance of $M_{t\bar{t}}$ for the higher mass Z'. Furthermore, large couplings are allowed at the 1σ level. However, note that the unitarity constraint derived for the process $u\bar{u} \to Z' \to t\bar{t}$ requires $|f_R| \lesssim 28$; see Appendix A for further details. Now, the heavy Z' contributions are very sensitive to width effects. For $f_L = g_L = 10$ we obtain $\Gamma_{Z'} \simeq 0.55 m_{Z'}$. The positive contributions to the $M_{t\bar{t}}$ distribution, particularly in its last bin, are somewhat constrained. We conclude that this model can offer a small improvement over the SM in describing $A_{\text{FB}}^{\text{tot}}$, $\sigma_{t\bar{t}}^{\text{tot}}$, and the $t\bar{t}$ invariant mass distribution simultaneously.

VI. FLAVOR-VIOLATING Z' AND $W'^{\pm}$ MODELS

In this section we consider a flavor-violating Z' model, which includes a u-t-Z' interaction. Such a flavor-changing-neutral current (FCNC)could appear at tree level or loop level. Rather than focus on a specific model, we consider the following effective coupling of u-t-Z' [9]:

$$\mathcal{L} = e\bar{u}\gamma^{\mu}(f_L P_L + f_R P_R) t Z'_{\mu}, \tag{51}$$

where e denotes the electromagnetic coupling strength. In addition to the SM QCD production channel, $u\bar{u} \to g \to t\bar{t}$, the top quark pair can also be produced via the process $u\bar{u} \to t\bar{t}$ with a t channel Z' boson propagator. The top quark asymmetry is naturally generated by this new process which also interferes with the SM production mode. Therefore, the differential cross section versus the cosine of the top production angle is θ given as follows [10]:

$$\frac{d\hat{\sigma}}{d\cos\theta} = \mathcal{A}_{\text{SM}} + \mathcal{A}_{\text{INT}}^{Z'} + \mathcal{A}_{\text{NP}}^{Z'}, \tag{52}$$

where

$$\mathcal{A}_{\text{INT}}^{Z'} = \frac{\beta}{72\pi\hat{s}} \frac{e^2 g_s^2 (g_L^2 + g_R^2)}{\hat{s}(t - M_{Z'}^2)} \Big[2(\hat{u} - m_t^2)^2 + 2\hat{s}m_t^2 + \frac{m_t^2}{M_{Z'}^2}((t - m_t^2)^2 + \hat{s}m_t^2) \Big], \tag{53}$$

$$\mathcal{A}_{\text{NP}}^{Z'} = \frac{\beta}{128\pi\hat{s}} \frac{e^4}{(t - M_{Z'}^2)^2} \Big\{ 4[(g_L^4 + g_R^4)(\hat{u} - m_t^2)^2 + 2g_L^2 g_R^2 \hat{s}(\hat{s} - 2m_t^2)] + \frac{m_t^4}{M_{Z'}^4}(g_L^2 + g_R^2)^2 \times (4\hat{s}M_{Z'}^2 + (t - M_{Z'}^2)^2) \Big\}, \tag{54}$$

and $\mathcal{A}_{\text{SM}}$ is given in Eq. (20). The interference between the QCD and electroweak processes can be easily understood as follows. The $SU(N)$ gluon propagator can be split into a $U(N)$ gluon propagator and a $U(1)$ gluon propagator [47],

$$\sum_a t_{ij}^a t_{kl}^a = \frac{1}{2}\Big(\delta_{il}\delta_{kj} - \frac{1}{N}\delta_{ij}\delta_{kl}\Big), \tag{55}$$

where the $U(1)$ gluon, carrying a factor $1/N$, is unphysical. The color flow of the SM QCD channel (i.e., $u \to t$ and $\bar{t} \to \bar{u}$) is then exactly the same as the Z' induced t-channel diagram, resulting in interference between both processes.

Within the SM, the FCNC coupling u-t-Z vanishes at tree level, but can be generated at one loop. However, the one-loop generated coupling is strongly suppressed by the GIM mechanism, making the FCNC top interactions very small. In models beyond the SM this GIM suppression can be relaxed, and one-loop diagrams mediated by new particles may also contribute, yielding effective couplings orders of magnitude larger than those of the SM. Since the coupling strength of this FCNC interaction is typically at the order of the SM weak interaction, the coefficients f_L and f_R are expected to be much smaller than 1. Therefore, it is not easy to generate a large asymmetry from a loop-induced u-t-Z interaction. However, the couplings f_L and f_R could be larger if they are generated at tree level.

While the value of f_R is not well constrained by direct or indirect search experiments, the value of f_L is tightly bounded by the B sector. The left-handed coupling f_L in Eq. (51) originates from the gauge interaction of the Z' boson to the first and third generation quark doublets,

$$\mathcal{L} = \bar{q}_L i\gamma^{\mu} D_{\mu} Q_L + \text{H.c.}, \tag{56}$$

where $q_L(Q_L)$ denotes the first (third) generation quark doublet and the covariant derivative is $D_{\mu} = i\partial_{\mu} + iB'Z'_{\mu}$, where B' is the charge. The flavor-violating interaction d_L-b_L-Z' then follows directly from the gauge invariance, which can contribute to the B_d^0-$\bar{B}_d^0$ mixing at the tree level.[2] A coupling of the form

$$\mathcal{L} = e\bar{d}\gamma^{\mu}(f_L V_{ud}^* V_{tb} P_L) b Z'_{\mu}, \tag{57}$$

follows from Eq. (56) after rotating to the mass eigenstate basis with f_L as in Eq. (51) and V_{ud} and V_{tb} elements of the Cabibbo-Kobayashi-Maskawa matrix. Assuming no additional NP effects arise, this gives a contribution to the mass difference between B_d^0-$\bar{B}_d^0$ of

$$\Delta m = \frac{4e^2 f_L^2}{3} |V_{ud}^* V_{tb}|^2 \frac{f_{B_d}^2 \hat{B} M_{B_d}}{M_{Z'}^2} \tag{58}$$

where f_{B_d} is the B_d decay constant and $\hat{B}$ is the "bag parameter" that characterizes the deviation from the vacuum saturation approximation. If we conservatively require that this contribution does not exceed the experimental value of 3.34×10^{-10} MeV [49], we can set a limit on f_L of

[2] A similar correlation among the gauge boson and the third generation quarks in the SM has been studied in Ref. [48].

$$f_L < 3.5 \times 10^{-4}\left(\frac{M_{Z'}}{100\ \text{GeV}}\right), \tag{59}$$

where we use $f_{B_d}\sqrt{\hat{B}} = 216 \pm 15$ MeV [50] and $|V_{ud}^* V_{tb}| \simeq 1$ [49]. As a result, we choose $f_L = 0$ hereafter. Furthermore, the unitarity constraint derived for the process $u\bar{t} \to Z' \to \bar{u}t$ requires only $|f_R| \lesssim 28$; see Appendix A for further details.

The most striking signal of the FCNC Z' model is same-sign top pair production through the processes $uu \to tt$ via a t-channel diagram mediated by the Z' boson. Recently, the CDF Collaboration searched for the same-sign top pair signature induced by the maximally flavor-violating scalars at the Tevatron and found no evidence of new physics beyond the SM [51]. In their analysis, the upper limit to the production cross section of same-sign top pairs is of the order of 0.7 pb. We show, in Fig. 15, the same-sign top production cross section at the Tevatron for couplings $f_R = 1$ and $f_L = 0$. The cross section scales with the right coupling as $\sigma(tt + \bar{t}\,\bar{t}) \sim f_R^4$ if $f_L = 0$. Direct production via t-channel Z' exchange dominates and is severely constrained as the couplings increase. Note that we do not consider the possible effects that same-sign top production could have on a measurement of A_{FB}, which requires a delicate analysis and will be presented elsewhere [52].

In Fig. 16, we show the result of the MCMC scan in the plane of $m_{Z'}$ and f_R: (a) for the current integrated luminosity and (b) for expected 10 fb^{-1}. For the current integrated luminosity, we impose the constraint of $\sigma(tt + \bar{t}\,\bar{t}) < 0.7$ pb [51], whereas for 10 fb^{-1}, we assume the cross section limit scales with $1/\sqrt{\mathcal{L}}$, giving $\sigma(tt + \bar{t}\,\bar{t}) < 0.4$ pb. The value of $\langle\chi^2\rangle_{\text{chain}} = 1.90$ for the current integrated luminosity indicates that the FCNC Z' model fits $\sigma(t\bar{t})$, A_{FB}, and the $M_{t\bar{t}}$ distribution worse than the SM. Note the quality of fit is maintained even if we fix the Z' mass to be specific values as in the flavor-conserving G' and Z' cases. Since the INT effects lead to a negative asymmetry, one needs a large NPS contribution to overcome the negative INT contributions to generate the positive asymmetry. That requires a very large f_R coupling, as seen in the upper and lower 1σ contours of Figs. 16(a) and 16(b), which is near the constraint of $\sigma(tt + \bar{t}\,\bar{t}) < 0.7$ pb. In this model, the predicted value for the same-sign top pair production cross section is pushed to just below the limit taken. Overall, while there is tension between the positive asymmetry and small $\sigma(tt + \bar{t}\,\bar{t})$, we find a fit not much worse than the SM. With 10 fb^{-1}, the fit remains worse than in the SM with $\langle\chi^2\rangle_{\text{chain}} = 4.39$.

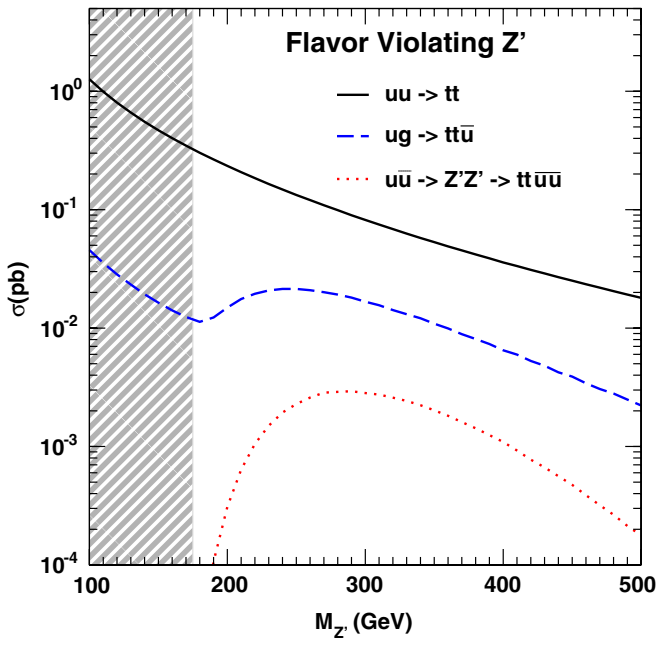

FIG. 15 (color online). Value of the same-sign top quark production cross section at the Tevatron for a flavor-violating Z' with $f_L = 0$, $f_R = 1$ (Eq. (51)).

The observed top asymmetry may also be induced by a flavor-changing interaction via a charged W' boson [10,18]. The top quark pair can be produced in the channel $d\bar{d} \to t\bar{t}$ via a t-channel W' boson propagator. As in the flavor-violating Z' case, we consider the following effective d-t-W' coupling:

$$\mathcal{L} = e\bar{d}\gamma^\mu(f_L P_L + f_R P_R)tW'_\mu, \tag{60}$$

where e denotes the electromagnetic coupling strength. The differential cross section of $d\bar{d} \to t\bar{t}$ is the same as Eq. (52) with the substitution $u(\bar{u}) \to d(\bar{d})$.

One advantage of the flavor-violating W' model is that it does not suffer from the constraint of same-sign top pair production at the Tevatron. Figure 17 displays the correlation between f_L and f_R couplings for a 2000 GeV W' boson. For the current luminosity the 1σ contours are symmetric for f_L and f_R, and the innermost one includes $f_L = f_R = 0$. In order to generate positive asymmetry, the couplings f_L and f_R need to be large enough to overcome the negative INT contributions. The typical values of couplings f_L and f_R are in the range of ± 10 to ± 20. For the current luminosity, $\langle\chi^2\rangle_{\text{chain}} = 1.67$, which indicates a better overall fit than the FCNC Z' boson due to the lack of the same-sign top constraint, and a better fit than the SM. Because of the PDF dependence, the d-quark initiated $t\bar{t}$ production via the W' is smaller than the u-quark initiated production through a Z'. Therefore, larger couplings are required to maintain the production cross section than in the Z' case. With upgraded luminosity, $\langle\chi^2\rangle_{\text{chain}} = 3.61$ provided that the central values of $A_{\text{FB}}^{\text{tot}}$ and $\sigma_{t\bar{t}}^{\text{tot}}$ are maintained which offers more improvement over the SM.

We focus on a heavy W' due to general constraints from electroweak precision and flavor measurements. In general, a W' is associated with a broken non-Abelian gauge group, and one must also consider a neutral gauge boson, Z', whose mass is typically degenerate or nearly so with that of the W'. If this Z' has predominantly flavor-changing couplings to top quarks, then it falls into the previous case

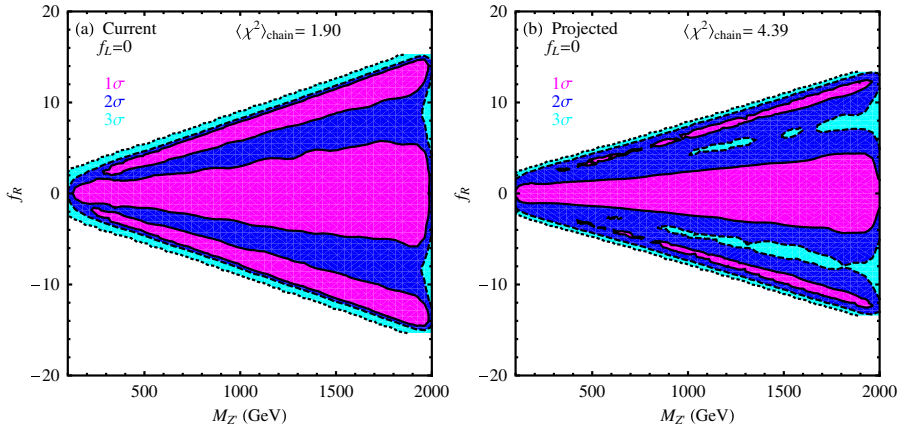

FIG. 16 (color online). Correlation of f_R and $m_{Z'}$ with $f_L = 0$. The left panel is for the current integrated luminosity while the right panel is for an upgraded luminosity of $\int \mathcal{L}dt = 10$ fb^{-1}. Tension with the same-sign top production constraint from the Tevatron prevents this model from becoming a better fit than the SM.

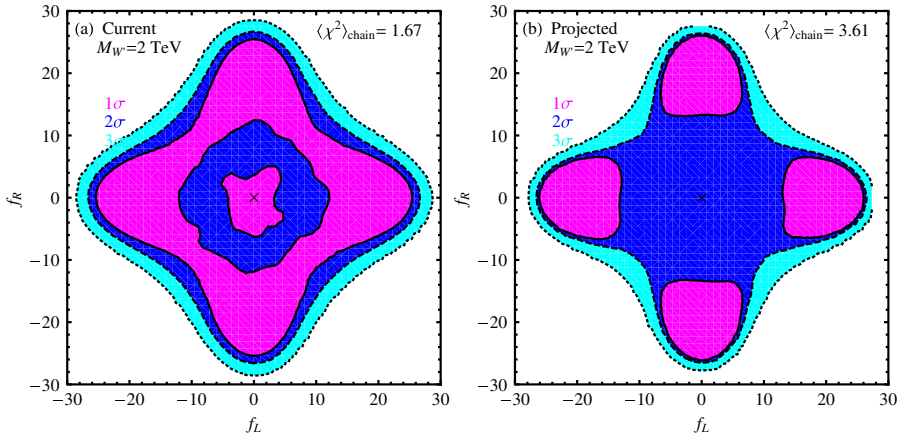

FIG. 17 (color online). Correlation of couplings for $m_{W'} = 2000$ GeV. The left panel is for the current integrated luminosity while the right panel is for an upgraded luminosity of $\int \mathcal{L}dt = 10$ fb^{-1}. The 1σ region is bounded by the solid curves, the 2σ by the dashed curves, and the 3σ by the dotted curves. Couplings of either $f_L \sim 0$ and $f_R \sim \pm 10$ or $f_R \sim 0$ and $f_L \sim \pm 10$ are consistent with the $A_{\rm FB}$ and $\sigma_{t\bar{t}}$ measurements.

we analyzed. If its coupling to top quarks is flavor-conserving then one would expect to produce top quark pairs through s-channel Z' exchange. However, such a process suffers from PDF suppression and is negligible in comparison to the W' contribution considered above and therefore we ignore it here.[3]

VII. FLAVOR-VIOLATING SCALAR $S/S^{\pm}$

In addition to spin-1 exchange, we also consider the FCNC top interaction with a new color singlet scalar S':

$$\mathcal{L} \supset eS'(f_L \bar{u}_R t_L + f_R \bar{u}_L t_R), \tag{61}$$

where S' is an $SU(2)$ doublet and we parameterize the overall coupling strength with respect to the weak coupling e. If we assume S' to be the SM Higgs boson, then the FCNC top interaction originates from the dimension-six operator

$$\mathcal{L} = \frac{v^2}{\Lambda^2} h(f_L \bar{u}_R t_L + f_R \bar{u}_L t_R).$$

Results for this operator can be obtained from those for Eq. (61) with the substitution $e \to \frac{v^2}{\Lambda^2}$. As will be shown below, such an effective coupling is too small to generate a sizable asymmetry, however. Hence, it is difficult to explain the asymmetry with the SM Higgs boson effective coupling without introducing additional heavy scalars.

The differential cross section is written as

$$\frac{d\hat{\sigma}}{d\cos\theta} = \mathcal{A}_{\rm SM} + \mathcal{A}^{S'}_{\rm INT} + \mathcal{A}^{S'}_{\rm NPS}, \tag{62}$$

[3]A model with a light W' and Z' has been proposed in Ref. [18] and may lead to a naturally good fit. This model has potential implications for precision electroweak observables which have not yet been fully explored.

where

$$\mathcal{A}^{S'}_{\rm INT} = \frac{2\pi\alpha_s\alpha_{\rm em}\beta(f_L^2+f_R^2)[\hat{s}m_t^2+(\hat{t}-m_t^2)^2]}{9\hat{s}^2(\hat{t}-m_{S'}^2)}, \quad (63)$$

$$\mathcal{A}^{S'}_{\rm NPS} = \frac{\pi\alpha_{\rm em}^2\beta(f_L^2+f_R^2)^2(\hat{t}-m_t^2)^2}{8\hat{s}(\hat{t}-m_{S'}^2)^2}, \quad (64)$$

with $\alpha_{\rm em} \equiv e^2/(4\pi)$. Because of the repulsive scalar interaction, the NPS contributions generate a negative $A_{\rm FB}^{\rm NP}$. In order to generate a positive $A_{\rm FB}^{\rm NP}$, the scalar S' needs to be very light, generally $m_{S'} < m_t$, and to have large couplings with the top quark. However, such a light scalar leads to a new top quark decay channel $t \to S'u$, which is tightly constrained [49]. Therefore, we consider scalar masses that are larger than top quark mass to forbid this new decay channel. Furthermore, the flavor-violating coupling will be highly constrained by D^0-$\bar{D}^0$ mixing (a $\Delta C = 2$ process) if one assumes a universal flavor-violating coupling among the three families of quarks. However, from a purely phenomenological perspective, we assume that the second generation quarks are not involved in the flavor-violating Yukawa interaction which leads to no constraint on the Yukawa couplings f_L and f_R. In other words, f_{ut} (f_L, f_R) is taken as a free parameter and is only constrained by considerations of unitarity (see Appendix A for details).

We plot $A_{\rm FB}^{\rm NP}$ as a function of $f = \sqrt{f_L^2+f_R^2}$ for a scalar of mass 2 TeV in Fig. 18(d) and see that it is indeed negative. This does not pose a problem with respect to the measurement of a positive asymmetry since the scalar interferes destructively with the SM which gives a negative R, defined in Eq. (6) and shown in Fig. 18(c). Thus, the total asymmetry, which is related to $A_{\rm FB}^{\rm NP}$ and R in Eq. (5), is positive. This is plotted in Fig. 18(a).

We also consider a charged scalar, $S^{\pm}$, which couples to top quarks as in Eq. (61), but with the replacement $u \to d$. In Fig. 19, we see the result of the MCMC scan in the plane of f_L and f_R for a 1000 GeV neutral S' and charged $S^{\pm}$ scalar: (a,c) for the current luminosity and (b,d) for expected 10 fb^{-1}, again assuming the central value of experimental data is not changed. For the neutral scalar, we impose the same-sign top pair production constraint discussed in Sec. VI. We plot the same-sign top pair production cross section for a neutral scalar with $f_L = f_R = 1$ at the Tevatron in Fig. 20. In the case of the neutral scalar, with the current luminosity we find a marginally better fit than in the SM, $\langle\chi^2\rangle_{\rm chain} = 1.72$. The fit improves relative to the SM with $\langle\chi^2\rangle_{\rm chain} = 3.15$ for 10 fb^{-1} if the central values remain the same. For the charged scalar we obtain a similar fit at the current luminosity with $\langle\chi^2\rangle_{\rm chain} = 1.72$. At 10 fb^{-1} with the same central values we obtain a slightly better fit, $\langle\chi^2\rangle_{\rm chain} = 3.04$, than in the case of the neutral scalar due to differences between the u and d PDFs. Although the negative $\sigma_{\rm INT}$ decreases the total cross section $\sigma_{t\bar{t}}$, it allows for good agreement with the $\frac{d\sigma}{dM_{t\bar{t}}}$ distribution and gives a positive contribution to $A_{\rm FB}^{\rm tot}$, which results in a better overall fit.

VIII. CONCLUSION

We have examined a number of models for new physics in top quark pair production which could account for the

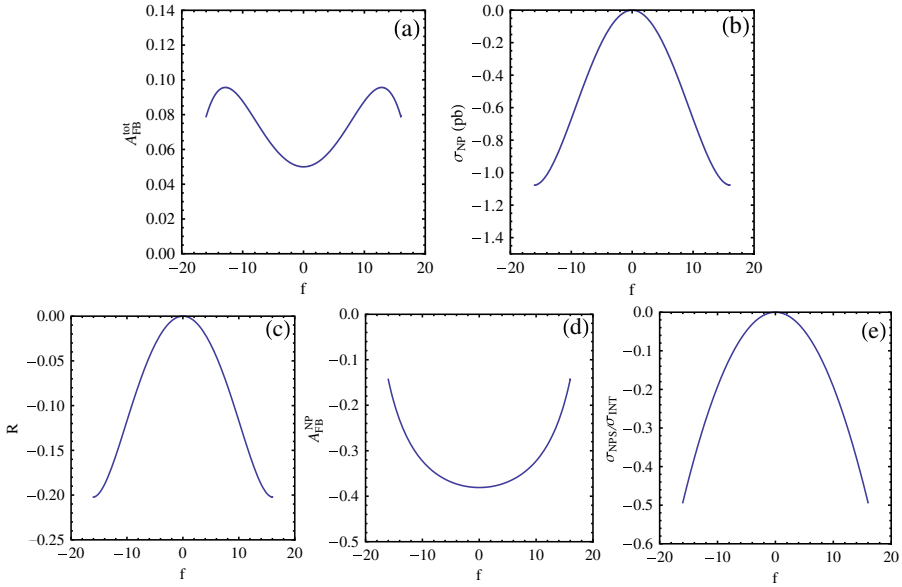

FIG. 18 (color online). Theoretical expressions for a flavor-violating neutral scalar S. (a) $A_{\rm FB}^{\rm tot}$ [cf. Eqs. (3)–(5)] as a function of $f = \sqrt{f_L^2+f_R^2}$ for a flavor-violating scalar with $m_S = 2$ TeV. (b) $\sigma_{\rm NP} = \sigma_{\rm INT} + \sigma_{\rm NPS}$ vs f. Note that the interference is destructive. (c) R, as defined in Eq. (6). Note that it is negative for all f. (d) $A_{\rm FB}^{\rm NP}$ vs f which is negative, as mentioned in the text. (e) The ratio of $\sigma_{\rm NPS}$ to $\sigma_{\rm INT}$. The INT term dominates over the NPS term for a scalar of mass 2 TeV.

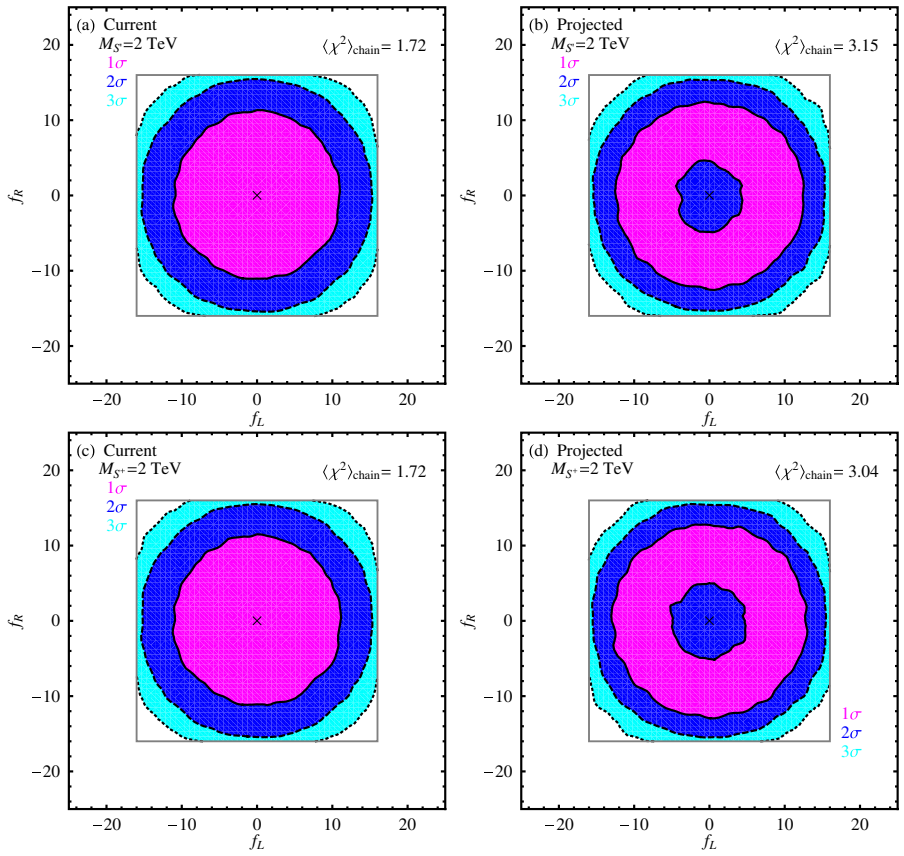

FIG. 19 (color online). Correlation of couplings for (a,b) $m_{S'} = 2000$ GeV and (c,d) $m_{S^\pm} = 2000$ GeV. The left panels are for the current integrated luminosity while the right panels are for an upgraded luminosity of $\int \mathcal{L} dt = 10$ fb^{-1}. The regions of each figure, from innermost to outermost, are (a) within 1σ, within 2σ, within 3σ, and greater than 3σ; (b) within 2σ, within 1σ, within 2σ, within 3σ, and greater than 3σ; (c) within 1σ, within 2σ, within 3σ, and greater than 3σ; (d) within 2σ, within 1σ, within 2σ, within 3σ, and greater than 3σ. The couplings are varied only within their allowed values from unitarity considerations (see Appendix A).

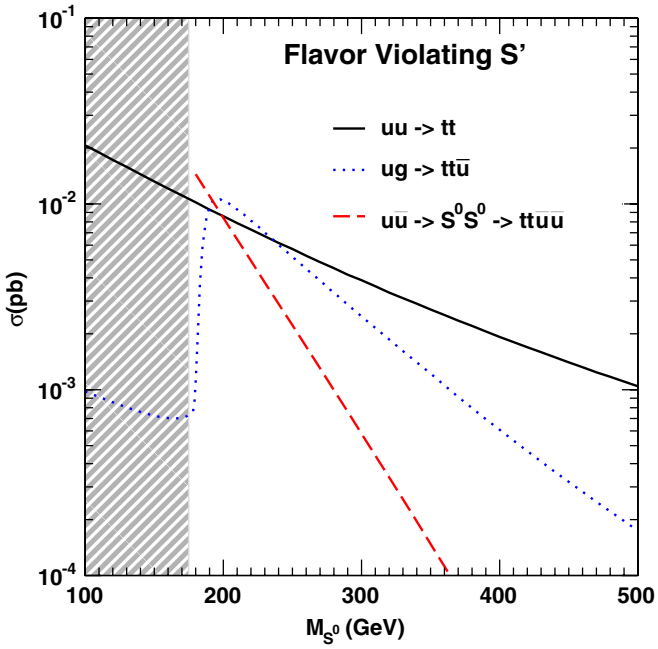

FIG. 20 (color online). Value of the same-sign top quark production cross section at the Tevatron for a flavor-violating S' with $f_L = f_R = 1$ [Eq. (61)]. The gray region indicates $m_{S'} < m_t$.

larger-than-expected forward-backward asymmetry observed at the Fermilab Tevatron, while not significantly disturbing the approximate agreement of the cross section $\sigma_{t\bar{t}}$ and its $M_{t\bar{t}}$ distribution with the standard model predictions. Our results are summarized in Table IV.

The results summarized in Table IV show that it is not easy to account for the larger-than-expected value of $A_{\rm FB}(t\bar{t})$ observed at the Fermilab Tevatron while maintaining the good agreement between theory and experiment for the production cross section $\sigma_{t\bar{t}}$ and differential rate $\frac{d\sigma}{dM_{t\bar{t}}}$.

Of the models considered, those that provide a fit better than the SM for the applicable data are a 1 TeV or 2 TeV flavor-conserving G' with axial couplings, a 2 TeV W' (or a 2 TeV flavor-conserving G' or Z') with chiral couplings. Other models we considered provide at most a mild improvement with respect to the SM case. The 1 TeV cases often give large corrections to the $M_{t\bar{t}}$ distribution since the additional signal is well inside the data region. Finally, in Table V, we examine in detail the contribution to the $\langle\chi^2\rangle_{\rm chain}$ in the small neighborhood around the best points in parameter space of the axial G', chiral G', FV chiral W', and FC chiral Z' models as well as the SM. Assuming the

TABLE IV. Models for top quark pair production and their ability to account simultaneously for the cross section and forward-backward asymmetry in top quark pair production at the Tevatron. FC and FV models are considered.

Model	Result	
FC G'	1 TeV	Poor fit for $f_R = g_R = 0$ considered due to $\frac{d\sigma}{dM_{t\bar{t}}}$ constraint; Good fit for axial couplings
	2 TeV	Fit not significantly improved with respect to the SM for $f_R = g_R = 0$; Excellent fit for axial couplings
EFT		Poor fit; $A_{\rm FB}$ consistently smaller than measured value.
FC Z'	1 TeV	Poor fit due to $\frac{d\sigma}{dM_{t\bar{t}}}$ constraint
	2 TeV	Fit not significantly improved with respect to the SM for $f_R = g_R = 0$
FV Z'		Poor fit due to $\frac{d\sigma}{dM_{t\bar{t}}}$ constraint and same-sign top constraint
FV W'	2 TeV	Good fit although large couplings necessary with a large amount of fine-tuning
FV S', $S^{\pm}$	2 TeV	Tension with small predicted $\sigma_{t\bar{t}}$ leads to poor fit with current data; however, a good fit would be obtained if central values were unchanged after 10 fb^{-1}

current integrated luminosity for each measurement and a mass of the new states responsible for the $A_{\rm FB}$ deviation of 2 TeV, we find:

(i) The 2 TeV axial G' model provides the best overall fit to the experimental data considered in this article. It improves the agreement with experiment of both the total top quark production cross section and the forward-backward asymmetry. The fit to the $M_{t\bar{t}}$ distribution is slightly worse than in the SM case but still in good agreement with data.

(ii) The 2 TeV W' can also lead to a good fit to the data. It is able to generate a large asymmetry and to improve the agreement of total cross section with data without disturbing the differential cross section sizably for some regions of parameter space. However, large couplings are needed. Note that in Table V, the best-fit point in the W' case has a lower χ^2 than the axial G' although the $\langle\chi^2\rangle_{\rm chain}$ is lower for the axial G' indicating that the axial G' gives a better overall fit. Stated differently, the W' requires a greater amount of fine-tuning of its parameters to fit the data than the axial G'. This is seen in the large value of $\delta\langle\chi^2\rangle_{\rm point}$; a slight perturbation of the best-fit points greatly decreases the quality of the fit. The W' model provides such a large value since the χ^2 contributions from $\sigma_{t\bar{t}}$ and $A_{\rm FB}$ are aligned and increase together with couplings that deviate from the minimum χ^2 couplings. This is to be contrasted with the other models in which the increasing χ^2 contribution from, say, $A_{\rm FB}$ is compensated by a smaller χ^2 contribution from $\sigma_{t\bar{t}}$, resulting in a total χ^2 value that remains relatively flat.

(iii) The 2 TeV chiral G' and Z' do not lead to significant improvement over the SM. They reduce the discrepancy with the asymmetry measurement although they are unable to reduce it below 2σ without disturbing the $M_{t\bar{t}}$ distribution due to their large widths.

(iv) The 2 TeV FV scalars S' and $S^{\pm}$ have fits that are not significantly improved with respect to the SM. They lead to a significant discrepancy in $\sigma_{t\bar{t}}$ and only slightly improve the fit to $A_{\rm FB}$ and $d\sigma/dM_{t\bar{t}}$ with respect to the SM.

In this work, we have used the full NLO QCD $t\bar{t}$ production cross section. It is worth noting that partial NNLO QCD corrections to the $t\bar{t}$ cross section have been calculated in Ref. [24] and give rise to an enhancement of the total cross section of about 0.3 pb. This indicates that higher order QCD corrections might improve the agreement between the measured total cross section and its value in the SM, and therefore areas of NP parameter space

TABLE V. Values of χ^2 for selected models. Assuming the current integrated luminosities, the $\langle\chi^2\rangle_{\rm point}$ contributions from the production cross section, forward-backward asymmetry and invariant mass distribution in top quark pair production at the Tevatron are given for the chain only in the small neighborhood of the points that provide the best fit to the data in each model. The value of $\langle\chi^2\rangle_{\rm point}$ is the Total/$N_{\rm dof}$, where $N_{\rm dof} = 3$, and provides a measure of how well the best-fit point in each model fits the data. The value $\delta\langle\chi^2\rangle_{\rm point}$ is the $\langle\chi^2\rangle_{\rm point}$ value of a box that is $\pm 10\%$ wide in the couplings for the best-fit point and is a rough measure of fine-tuning. Note the SM value for $\langle\chi^2\rangle_{\rm point}$ is equivalent to that given in Eq. (15). The $\langle\chi^2\rangle_{\rm chain}$ values for each model are also listed.

Model	$\sigma_{t\bar{t}}$	$A_{\rm FB}$	$\frac{d\sigma}{dM_{t\bar{t}}}$	Total	$\langle\chi^2\rangle_{\rm point}$	$\delta\langle\chi^2\rangle_{\rm point}$	$\langle\chi^2\rangle_{\rm chain}$
FV W' ($f_L = 17.0$, $f_R = 0.0$, $m_{W'} = 2$ TeV):	0.63	0.06	0.27	0.96	0.32	41.4%	1.67
Axial G' ($f = 2.5$, $g = -2.5$, $m_{G'} = 2$ TeV):	0.75	0.47	0.75	1.97	0.66	1.6%	1.15
Chiral G' ($f_L = 2.0$, $g_L = -2.0$, $m_{G'} = 2$ TeV):	0.59	2.91	0.62	4.12	1.37	0.4%	1.69
FC Z' ($f_L = 8.0$, $g_L = 8.0$, $m_{Z'} = 2$ TeV):	0.67	2.66	0.91	4.24	1.41	1.0%	1.62
FV S' ($f_L = 7.0$, $f_R = 0.0$, $m_{S'} = 2$ TeV):	2.01	2.85	0.09	4.96	1.65	0.2%	1.72
FV $S^{\pm}$ ($f_L = 7.5$, $f_R = 0.0$, $m_{S'} = 2$ TeV):	2.01	2.85	0.12	4.98	1.66	0.2%	1.72
SM :	1.12	4.07	0.06	5.25	1.75	-	1.75

which give negative contributions to the total cross section will be less constrained. Such negative contributions, however, may be in tension with the observed $M_{t\bar{t}}$ invariant mass distribution. A detailed collider simulation, including the complete NNLO corrections, would be therefore highly desirable in order to make a more reliable comparison of the predictions of these models with data.

Crucial to the test of any model is also the accumulation of more integrated luminosity at the Tevatron, in order to demonstrate deviations from the standard model exceeding 3σ. Until then, the observed $A_{\rm FB}$ values cannot be regarded as anything more than a hint of new physics.

ACKNOWLEDGMENTS

Q.-H. C. is supported in part by the Argonne National Laboratory and University of Chicago Joint Theory Institute (JTI) under Grant No. 03921-07-137, and by the U.S. Department of Energy under Grant Nos. DE-AC02-06CH11357 and DE-FG02-90ER40560. D. M. and J. L. R. are supported by the U. S. Department of Energy under Grant No. DE-FG02-90ER40560. G. S. is supported in part by the U. S. Department of Energy under Grants Nos. DE-AC02-06CH11357 and DE-FG02-91ER40684. C. E. M. W. is supported in part by U.S. Department of Energy under Grant Nos. DE-AC02-06CH11357 and DE-FG02-90ER40560. J. L. R., G. S., and C. E. M. W. thank the Aspen Center for Physics for hospitality. The authors thank M. Neubert for useful discussions.

APPENDIX A: UNITARITY CONSTRAINTS

In this appendix, we explore the unitarity constraints on new physics models considered in this work. The weak isospin amplitude $\mathcal{M}^I$ (I being isospin index) can be decomposed with respect to orbital angular momentum according to

$$\mathcal{M}^I = 16\pi \sum_0^\infty (2\ell+1) P_\ell(\cos\theta) a_\ell^I. \tag{A1}$$

With the normalization $\Im a_\ell^I = |a_\ell^I|^2$, the unitarity constraint requires

$$|\Re a_\ell^I| < \tfrac{1}{2}, \tag{A2}$$

where a_ℓ^I could be projected via:

$$a_\ell^I = \frac{1}{32\pi} \int_{-1}^{1} d\cos\theta P_\ell(\cos\theta) \mathcal{M}^I. \tag{A3}$$

First consider the flavor-conserving Z' models, which involve the s-channel diagram only. Note that the constraints of the G' model can be easily derived from flavor-conserving Z' model. The helicity amplitudes for $q\bar{q} \to t\bar{t}$ are represented by $A(\lambda_q, \lambda_{\bar{q}}, \lambda_t, \lambda_{\bar{t}})$, where $\lambda_t = -, +$, respectively, indicates a left-handed and a right-handed top quark. Apart from the common factor

$$\frac{2e^2 E}{s - m_{Z'}^2},$$

the nonvanishing helicity amplitudes from the diagram mediated by the Z' boson are

$$A(-,+,-,-) = f_L \sin\theta m_t [g_L + g_R], \tag{A4}$$

$$A(-,+,-,+) = -f_L(1+\cos\theta)E[(1+\beta_t)g_L + (1-\beta_t)g_R], \tag{A5}$$

$$A(-,+,+,-) = f_L(1-\cos\theta)E[(1-\beta_t)g_L + (1+\beta_t)g_R], \tag{A6}$$

$$A(-,+,+,+) = -f_L \sin\theta m_t [g_L + g_R], \tag{A7}$$

$$A(+,-,-,-) = f_R \sin\theta m_t [g_L + g_R], \tag{A8}$$

$$A(+,-,-,+) = f_R(1-\cos\theta)E[(1+\beta_t)g_L + (1-\beta_t)g_R], \tag{A9}$$

$$A(+,-,+,-) = -f_R(1+\cos\theta)E[(1-\beta_t)g_L + (1+\beta_t)g_R], \tag{A10}$$

$$A(+,-,+,+) = -f_R \sin\theta m_t [g_L + g_R], \tag{A11}$$

where $\beta_t = \sqrt{1 - m_t^2/E^2}$. In the c.m. frame of the $t\bar{t}$ pair the 4-momenta of the particles are chosen to be

$$p_q = E(1,0,0,1), \tag{A12}$$

$$p_{\bar{q}} = E(1,0,0,-1), \tag{A13}$$

$$p_t = E(1, \beta_t \sin\theta, 0, \beta_t \cos\theta), \tag{A14}$$

$$p_{\bar{t}} = E(1, -\beta_t \sin\theta, 0, -\beta_t \cos\theta). \tag{A15}$$

In the high energy limit $E \gg m_t$, only $(1+\beta_t)$ terms contribute. The $J=1$ partial wave of the $A(-,+,-,+)$ amplitude is

$$a_s^{J=1}(q\bar{q} \to Z' \to t\bar{t}) = \frac{\alpha_{\rm em}}{12} f_L g_L, \tag{A16}$$

yielding the following limit $|f_L g_L| \leq 6/\alpha_{\rm em}$. Similarly, one can derive the following constraints

$$|f_L| \lesssim 28 \quad \text{and} \quad |g_L| \lesssim 28$$

from the $q\bar{q} \to Z' \to q\bar{q}$ and $t\bar{t} \to Z' \to t\bar{t}$ processes.

Now consider the flavor-violating Z' model. We consider the scattering $u\bar{t} \to Z' \to t\bar{u}$, the calculation of which is identical to the flavor-conserving Z' model. In the high energy limit $\sqrt{s} \gg m_t$, we obtain the following unitarity bound on f_R from the helicity amplitude $A(+,-,+,-)$ in Eq. (A10),

$$|f_R| \lesssim 28. \tag{A17}$$

Finally, we consider the scattering $u\bar{t} \to S \to \bar{u}t$ to derive the unitarity constraint for the flavor-violating S model. The helicity amplitudes are represented by $A(\lambda_q, \lambda_{\bar{t}}, \lambda_{\bar{u}}, \lambda_t)$. In the high energy limit $s \gg m_t$, the nonvanishing helicity amplitudes are

$$A(+,+,+,+) = e^2 f_R^2, \tag{A18}$$

$$A(+,+,-,-) = e^2 f_R f_L, \tag{A19}$$

$$A(-,-,+,+) = e^2 f_L f_R, \tag{A20}$$

$$A(-,-,-,-) = e^2 f_L^2, \tag{A21}$$

where f_L and f_R are given in Eq. (61). The $J = 0$ partial wave of $A(+,+,+,+)$ is

$$a_s^{J=0}(u\bar{t} \to S \to \bar{u}t) = \frac{\alpha_{\rm em}}{4} f_R^2, \tag{A22}$$

yielding the unitarity limit $f_L^2 \leq 2/\alpha_{\rm em}$. Hence, $|f_L| \lesssim 16$, $|f_R| \lesssim 16$, and $|f_L f_R| < 256$.

[1] G. Strycker *et al.* (CDF Collaboration) (2009) public note: CDF/ANAL/TOP/PUBLIC/9724, http://www-cdf.fnal.gov/physics/new/top/confNotes/cdfnote_9724_public_v01-3.pdf
[2] T. Aaltonen *et al.* (CDF Collaboration), Phys. Rev. Lett. **101**, 202001 (2008).
[3] O. Antunano, J. H. Kühn, and G. Rodrigo, Phys. Rev. D **77**, 014003 (2008).
[4] V. M. Abazov *et al.* (D0 Collaboration), Phys. Rev. Lett. **100**, 142002 (2008).
[5] J. H. Kühn and G. Rodrigo, Phys. Rev. Lett. **81**, 49 (1998).
[6] J. H. Kühn and G. Rodrigo, Phys. Rev. D **59**, 054017 (1999).
[7] A. Djouadi, G. Moreau, F. Richard, and R. K. Singh, arXiv:0906.0604.
[8] P. Ferrario and G. Rodrigo, Phys. Rev. D **80**, 051701 (2009).
[9] S. Jung, H. Murayama, A. Pierce, and J. D. Wells, Phys. Rev. D **81**, 015004 (2010).
[10] K. Cheung, W.-Y. Keung, and T.-C. Yuan, Phys. Lett. B **682**, 287 (2009).
[11] P. H. Frampton, J. Shu, and K. Wang, Phys. Lett. B **683**, 294 (2010).
[12] J. Shu, T. M. P. Tait, and K. Wang, Phys. Rev. D **81**, 034012 (2010).
[13] A. Arhrib, R. Benbrik, and C.-H. Chen, arXiv:0911.4875.
[14] P. Ferrario and G. Rodrigo, arXiv:0912.0687.
[15] I. Dorsner, S. Fajfer, J. F. Kamenik, and N. Kosnik, Phys. Rev. D **81**, 055009 (2010).
[16] D.-W. Jung, P. Ko, J. S. Lee, and S.-h. Nam, arXiv:0912.1105.
[17] J. Cao, Z. Heng, L. Wu, and J. M. Yang, Phys. Rev. D **81**, 014016 (2010).
[18] V. Barger, W.-Y. Keung, and C.-T. Yu, arXiv:1002.1048.
[19] CDF Collaboration public note: http://www-cdf.fnal.gov/physics/new/top/2009/xsection/TopXsNN/topXs_46fb_public.html.
[20] CDF Collaboration public note: http://www-cdf.fnal.gov/physics/new/top/confNotes/cdf9913_ttbarxs4invfb.ps.
[21] P. M. Nadolsky *et al.*, Phys. Rev. D **78**, 013004 (2008).
[22] U. Langenfeld, S. Moch, and P. Uwer, Phys. Rev. D **80**, 054009 (2009).
[23] V. Barger, W.-Y. Keung, and G. Shaughnessy, Phys. Rev. D **78**, 056007 (2008).
[24] N. Kidonakis and R. Vogt, Phys. Rev. D **78**, 074005 (2008).
[25] P. Nason, S. Dawson, and R. K. Ellis, Nucl. Phys. **B303**, 607 (1988).
[26] W. Beenakker, H. Kuijf, W. L. van Neerven, and J. Smith, Phys. Rev. D **40**, 54 (1989).
[27] M. Cacciari, S. Frixione, M. L. Mangano, P. Nason, and G. Ridolfi, J. High Energy Phys. 09 (2008) 127.
[28] S. Moch and P. Uwer, Nucl. Phys. B, Proc. Suppl. **183**, 75 (2008).
[29] L. G. Almeida, G. Sterman, and W. Vogelsang, Phys. Rev. D **78**, 014008 (2008).
[30] T. Aaltonen *et al.* (CDF Collaboration), Phys. Rev. Lett. **102**, 222003 (2009).
[31] D0 Collaboration public note: http://www-d0.fnal.gov/Run2Physics/WWW/results/prelim/TOP/T83/T83.pdf.
[32] J. Pumplin *et al.*, J. High Energy Phys. 07 (2002) 012.
[33] J. C. Pati and A. Salam, Phys. Lett. **58B**, 333 (1975).
[34] L. J. Hall and A. E. Nelson, Phys. Lett. **153B**, 430 (1985).
[35] P. H. Frampton and S. L. Glashow, Phys. Lett. B **190**, 157 (1987).
[36] P. H. Frampton and S. L. Glashow, Phys. Rev. Lett. **58**, 2168 (1987).
[37] J. Bagger, C. Schmidt, and S. King, Phys. Rev. D **37**, 1188 (1988).
[38] F. Cuypers, Z. Phys. C **48**, 639 (1990).
[39] Q.-H. Cao, S.-L. Chen, E. Ma, and G. Rajasekaran, Phys. Rev. D **73**, 015009 (2006).
[40] C. D. Carone, J. Erlich, and M. Sher, Phys. Rev. D **78**, 015001 (2008).
[41] P. Ferrario and G. Rodrigo, Phys. Rev. D **78**, 094018 (2008).
[42] M. V. Martynov and A. D. Smirnov, Mod. Phys. Lett. A **24**, 1897 (2009).
[43] R. Contino, T. Kramer, M. Son, and R. Sundrum, J. High Energy Phys. 05 (2007) 074.
[44] J. M. Campbell and R. K. Ellis, Phys. Rev. D **62**, 114012 (2000).
[45] V. Ahrens, A. Ferroglia, M. Neubert, B. D. Pecjak, and L. L. Yang, Phys. Lett. B **687**, 331 (2010).
[46] J. L. Rosner, Phys. Lett. B **387**, 113 (1996).
[47] F. Maltoni, K. Paul, T. Stelzer, and S. Willenbrock, Phys. Rev. D **67**, 014026 (2003).
[48] E. L. Berger, Q.-H. Cao, and I. Low, Phys. Rev. D **80**,

074020 (2009).
[49] C. Amsler *et al.* (Particle Data Group), Phys. Lett. B **667**, 1 (2008).
[50] E. Gamiz, C. T. H. Davies, G. P. Lepage, J. Shigemitsu, and M. Wingate, Phys. Rev. D **80**, 014503 (2009).
[51] T. Aaltonen *et al.* (CDF Collaboration), Phys. Rev. Lett. **102**, 041801 (2009).
[52] Q.-H. Cao, D. McKeen, J. L. Rosner, G. Shaughnessy, and C. E. M. Wagner (unpublished).